UNIVERSITY OF CALIFORNIA, MERCED

Investigating the Molecular Mechanisms of Shear-Activated Chemical Reactions Using Reactive Molecular Dynamics Simulations

by

Fakhrul Hasan Bhuiyan

A dissertation submitted in partial satisfaction of the requirements for the degree of

Doctor of Philosophy

in

Mechanical Engineering

Committee in charge:

Professor Mehmet Z. Baykara, Chair

Professor Ashlie Martini, Advisor

Professor Liang Shi

Professor Min Hwan Lee

The Thesis of Fakhrul Hasan Bhuiyan is approved, and it is acceptable in quality and form for publication on microfilm and electronically:

Professor Mehmet Z. Baykara, Chair	Date
Professor Ashlie Martini, Advisor	Date
Professor Liang Shi	Date
Professor Min Hwan Lee	Date

University of California, Merced

2024

To my parents, for their lifelong dedication and sacrifices

My wife, Rafia, for her love and support

And my newborn son, Raeed, for bringing new colors to our life

Table of Contents

List of Figures

List of Tables

Acknowledgments

First, I would like to thank my Ph.D. advisor, Dr. Ashlie Martini, for her guidance and immense support. Dr. Martini is perhaps the best mentor I have met so far. I have also found her to be compassionate as a human, brilliant as a scientist, impeccable at communication, and highly professional. I have learned a great deal from her and developed most of my professional, communication, mentorship, soft, and technical skills under her watch. I am glad to have decided to join her group for my Ph.D.

I would also like to thank everyone in the Martini Research Group, former and current, with whom I had the pleasure to work with. Everyone in the group has been a great source of support, new learnings, and great ideas for me. Especially, I would like to mention Dr. Arash Khajeh for being my mentor at the start of my Ph.D., and Dr. Quanpeng Yang (Sam) for his support and guidance throughout my Ph.D. journey and beyond.

I want to thank our collaborator Dr. Seong H. Kim from Pennsylvania State University and his students Seokhoon Jang and Yu-Sheng Li. All ball-on-flat tribometer experiments and experimental characterizations discussed in this dissertation were performed by them. They are amazing scientists to work with. Their inputs, insights, and suggestions on our work have significantly improved the quality and impact of this dissertation.

This work was supported by the National Science Foundation (Grant No. CMMI-2038494 and 2038499). Simulations and data analysis were carried out using the MERCED and the Pinnacles clusters at UC Merced.

The text of this dissertation includes reprints of the following previously published material as they appear in:

- Bhuiyan, F. H., Li, Y. S., Kim, S. H., & Martini, A. (2024). Shear-Activation of Mechanochemical Reactions Through Molecular Deformation. Scientific Reports, 14, 2992.
- Bhuiyan, F. H., Li, Y. S., Kim, S. H., & Martini, A. (2023). Shear-Activated Chemisorption and Association of Cyclic Organic Molecules. Faraday Discussions, 241, 194-205.
- Bhuiyan, F. H., Kim, S. H., & Martini, A. (2022). Reactive Molecular Dynamics Simulations of Thermal and Shear-driven Oligomerization. Applied Surface Science, 591, 153209.

The co-authors listed in these publications directed and supervised research which forms the basis for the dissertation.

Curriculum Vita

Education

- Ph.D. in Mechanical Engineering, University of California, Merced, 2024
    - **Dissertation:** Investigating the Molecular Mechanisms of Shear-Activated Chemical Reactions Using Reactive Molecular Dynamics Simulations
    - **Supervisor:** Dr. Ashlie Martini
- M.S. in Mechanical Engineering, University of California, Merced, 2023
- B.Sc. in Mechanical Engineering, Bangladesh University of Engineering and Technology, 2018
    - **Thesis:** Molecular Dynamics Study of Mechanical Properties of a Solar Cell Structure Employing Silicon NanoRod under Uniaxial Compression
    - **Supervisor:** Dr. Md. Afsar Ali

Publications

- Cobeña-Reyes, J., **Bhuiyan, F. H.**, & Martini, A. (2024). Atomistic simulations of mechanically activated reactions for oxygen release from polymers. (in review)
- Faiyad, A., **Bhuiyan, F. H.**, Vellore, A., Johnson, D., Kennett, A., & Martini, A. (2024). Temperature-dependent Wear Life of MoS2 Dry Film Lubricants. (in review)
- Li, Y. S., **Bhuiyan, F. H.**, Kim, S. H., & Martini, A. (2024). Elucidating Tribochemical Reaction Mechanisms: Insights into Tribofilm Formation from Adsorbates Coupled with Tribochemical Substrate Wear. (in review)
- **Bhuiyan, F. H.**, Li, Y. S., Kim, S. H., & Martini, A. (2024). Shear-Activation of Mechanochemical Reactions Through Molecular Deformation. Scientific Reports, 14, 2992.
- Ogbomo, E., **Bhuiyan, F. H.**, Latorre, C. A., Martini, A., & Ewen, J. P. (2024). Effects of Surface Chemistry on the Mechanochemical Decomposition of Tricresyl Phosphate. Physical Chemistry Chemical Physics, 26(1), 278-292.
- Chen, L., Yan, W., **Bhuiyan, F. H.**, Tang, C., Jiang, Y., Jang, S., Liu, Y., Wu, J., Wang, W., Wang, Y., Zheng, J., Martini, A., Qian, L., & Kim, S. H. (2023). Understanding and Preventing Lubrication Failure at the Carbon Atomic Steps. Small, 2301515.
- Li, Y. S., Jang, S., **Bhuiyan, F. H.**, Martini, A., & Kim, S. H. (2023). Molecular Structure and Environment Dependence of Shear-driven Chemical Reactions: Tribopolymerization of Methylcyclopentane, Cyclohexane and Cyclohexane on Stainless Steel. Tribology Letters, 71(2), 49.
- **Bhuiyan, F. H.**, Li, Y. S., Kim, S. H., & Martini, A. (2023). Shear-Activated Chemisorption and Association of Cyclic Organic Molecules. Faraday Discussions, 241, 194-205.
- **Bhuiyan, F. H.**, Kim, S. H., & Martini, A. (2022). Reactive Molecular Dynamics Simulations of Thermal and Shear-driven Oligomerization. Applied Surface Science, 591, 153209.

- Khajeh, A., **Bhuiyan, F. H.**, Mogonye, J. E., Pesce-Rodriguez, R. A., Berkebile, S., & Martini, A. (2021). Thermal Decomposition of Tricresyl Phosphate on Ferrous Surfaces. The Journal of Physical Chemistry C, 125(9), 5076-5087.

Presentations

Oral Presentations

- **Bhuiyan, F. H.**, Li, Y. S., Kim, S. H., & Martini, A. "Shear-Activation of Mechanochemical Reactions Through Molecular Deformation", ACS Spring 2024, March 2024, New Orleans, LA.
- **Bhuiyan, F. H.**, Li, Y. S., Kim, S. H., & Martini, A. "Molecular Mechanisms of Tribochemical Reactions: Reactive Molecular Dynamics Simulations of Cyclic Organic Molecules", STLE 2023 Annual Meeting & Exhibition, May 2023, Long Beach, CA.
- **Bhuiyan, F. H.**, Li, Y. S., Kim, S. H., & Martini, A. "Molecular Mechanisms of Tribochemical Reactions: Reactive Molecular Dynamics Simulations of Cyclic Organic Molecules", Web Seminar Series on Tribology, October 2022, Remote Meeting.
- **Bhuiyan, F. H.**, & Martini, A. "Simulating Tribochemical Reactions with Molecular Dynamics and Improving Performance of Lubricant Additives", STLE Northern California Section Meeting, May 2022, Remote Meeting.
- **Bhuiyan, F. H.**, Li, Y. S., Kim, S. H., & Martini, A. "Reactive Molecular Dynamics Simulations of Thermal and Shear-Driven Tribopolymerization", STLE 2022 Annual Meeting & Exhibition, May 2022, Orlando, FL.
- **Bhuiyan, F. H.**, & Martini, A. "Reactive Molecular Dynamics Simulations of Tribochemical Reactions", The Pennsylvania State University, January 2022, State College, PA.

Poster Presentations

- **Bhuiyan, F. H.**, Li, Y. S., Kim, S. H., & Martini, A. "Molecular Mechanisms of Tribochemical Reactions: Reactive Molecular Dynamics Simulations of Cyclic Organic Molecules", STLE 2023 Annual Meeting & Exhibition, May 2023, Long Beach, CA.
- **Bhuiyan, F. H.**, Li, Y. S., Kim, S. H., & Martini, A. "Reactive Molecular Dynamics Simulations of Thermal and Shear-Driven Oligomerization", ACS Spring 2022, March 2022, San Diego, CA.

Awards and Honors

- PBGA Professional Development Award, *Division of Graduate Studies, University of California Merced*, Spring 2024
- Graduate Dean's Dissertation Fellowship, *Division of Graduate Studies, University of California Merced*, Spring 2024

- Campus Finalist in Grad Slam, A Research Presentation Competition, *Division of Graduate Studies, University of California Merced*, Spring 2023
- GRAD-EXCEL Peer Mentor Fellowship, *Division of Graduate Studies, University of California Merced*, Spring 2023
- ME Spring 2023 Travel Fellowship, *School of Engineering, University of California Merced*, Spring 2023
- ME Bobcat Travel Fellowship, *School of Engineering, University of California Merced*, Spring 2022
- Research Scholarship, Society of Tribologists and Lubrication Engineers (STLE) Northern California Section, January 2022
- ME Bobcat Fellowship, *School of Engineering, University of California Merced*, Spring 2022
- ME Travel Award, *School of Engineering, University of California Merced*, Spring 2022

Research Projects

- **Mechanochemical Reactions of Organic Compounds and Commercially Used Antiwear Additives**
    - Using reactive MD simulations and data analysis techniques to study the nanoscale mechanisms of mechanochemical reactions of simple organic molecules and commercially used antiwear additives, in collaboration with ball-on-flat tribometer experiments done by Dr. Seong Kim's group at PSU. (Jan 2021 - Current)
- **Temperature-Dependent Wear Life of MoS2 Dry Film Lubrication**
    - Performed reactive MD simulations of MoS_2 dry film coatings to investigate the temperature-dependent wear life of MoS2 coatings and complement experimental findings, in collaboration with ball-on-flat tribometer experiments done by NASA JPL. (Oct 2022 – Mar 2024)
- **Generative Large Language Model for Tribology**
    - Fine-tuned the OpenLLaMA 13B parameter model on a custom-made dataset consisting of tribology literature for summarizing, question-answering, and hypothesis-generation tasks. (Jun 2023 – Jan 2024)
- **Predicting Ionic Liquid Properties**
    - Scraped, cleaned, and preprocessed data from the NIST database on ionic liquids to train a graphical neural network for predicting ionic liquid properties based on the SMILES string. (Jun 2023 - Dec 2023)
- **Friction on Graphite Step-Edges**
    - Studied the friction and chemical reactivity on graphite using reactive MD simulations to identify different defects on graphite, in collaboration with atomic force microscopy experiments done by Dr. Seong Kim's group at PSU. (Jul 2021 - Jul 2022)
- **Structure of Adsorbed Water**
    - Analyzed the structure of adsorbed water layer on silica using reactive MD simulations and revealed a transition from water to ice-like structure near the surface. (Aug 2020 - Feb 2021)

- **Thermal Decomposition of Phosphorous-Based Lubricant Additives on Ferrous Surfaces**
    - Investigated the thermal decomposition reaction mechanisms of a commercially used antiwear additive, and the difference in reactivity of three isomers to elucidate the working principles of the antiwear additive, in collaboration with temperature-programmed reaction spectroscopy and gas chromatography-mass spectroscopy done by Army Research Lab. (Sep 2019 - Dec 2020)

Abstract

Shear-driven chemical reactions play a critical role in many manufacturing, tribological, and synthesis processes. However, mechanistic understanding of such reactions is still limited due to the inherent difficulty in studying shear-driven reactions using experimental techniques as these reactions often happen at a sliding interface. This dissertation aims to use reactive molecular dynamics (MD) to further the current understanding of shear-activation. First, we investigated the individual effects of heat, normal stress, and shear stress on reaction pathways using reactive MD simulations of α-pinene molecules on silica. Results identified shear stress as the key driver of oligomerization reactions under sliding conditions. Normal stress alone was ineffective in inducing any reactions and oligomerization could be driven thermally only at very high temperatures. Analysis of the reaction pathways showed that shear can activate multiple reaction mechanisms that are not accessible thermally. Calculations of bond lengths and dihedral angles revealed that such activations are associated with physical deformation of reacting species. Next, we studied shear-activated reactions of simple cyclic organic molecules to isolate the effect of chemical structure on reaction yield and pathway. Reactive MD simulations were used to model methylcyclopentane, cyclohexane, and cyclohexene subject to pressure and shear stress between silica surfaces. Cyclohexene was found to be more susceptible to undergo shear-activated oxidative chemisorption and subsequent oligomerization reactions than methylcyclopentane and cyclohexane. The oligomerization trend was consistent with shear-driven polymerization yield measured in ball-on-flat sliding experiments. Analysis of the reactants in simulations identified the C=C double bond in cyclohexene as being the origin of its shear susceptibility. Lastly, the most common reaction pathways for association were identified, providing insight into how the chemical structures of the precursor molecules determined their response to mechanochemical activation. Finally, we investigated the effect of molecular deformation on lowering the reaction energy barrier by studying the shear stress-driven oligomerization reactions of cyclohexene on silica using reactive MD simulations. Simulations captured an exponential increase in reaction yield with shear stress and highlighted the role of surface oxygen atoms in driving the reactions. Trends from simulations were corroborated by ball-on-flat tribometer experiments and elemental analysis of ball-on-flat reaction products. Structural analysis of the reacting molecules in simulations indicated the reactants were deformed just before a reaction occurred. Quantitative evidence of shear-induced deformation was established by comparing bond lengths in cyclohexene molecules in equilibrium and prior to reactions. Nudged elastic band calculations showed that the deformation had a small effect on the transition state energy but notably increased the reactant state energy, ultimately leading to a reduction in the energy barrier. Finally, a quantitative relationship was developed between molecular deformation and energy barrier reduction by mechanical stress. The findings from this dissertation on the activation mechanisms underlying shear-driven mechanochemical reactions provide critical insights that can guide design of materials and processes with optimized and potentially tunable shear-induced reactions.

1 Introduction

1.1 Mechanochemistry

1.1.1 Background

Mechanochemistry is the study of chemical reactions activated by mechanical force exerted on chemical species through processes such as grinding, milling, or shearing. Despite being an age-old concept, mechanochemical reactions have received less attention than other conventional reaction processes driven by heat, photons, or electrons. Recently, however, mechanochemistry has paved the way for many novel manufacturing, synthesis, and engineering processes that eliminate the need for a solvent, and thus, can be more energy efficient and safer than conventional technologies.[1–5] Other engineering applications where mechanochemistry plays a crucial role include surface functionalization,[6] chemical mechanical polishing,[7] polymer processing,[2,8] and tribology.[9,10] Depending on the application, the mechanical stress required to induce the relevant mechanochemical reactions can be provided through grinding, compression, tension, or shearing.

1.1.2 Theory (Bell Model)

The reaction kinetics of a mechanochemical reaction can be modeled using a stress-assisted thermal activation model, also commonly known as the Bell model.[11] According to the Bell model, the reaction rate constant of a mechanochemical reaction, *k*, can be described using a modified Arrhenius-like equation as,

$$k = A \exp\left(-\frac{E_a - E_m}{k_B T}\right) \tag{1}$$

where A is the pre-exponential factor, k_B is the Boltzmann constant, and T is the temperature, E_a is the thermal activation energy, and E_m is the mechanical energy which is a function of shear stress τ for shear-driven reactions as expressed by the following equation:

$$E_m = \tau \Delta V^* \tag{2}$$

where τ is shear stress and ΔV^* is the activation volume. Combining Equations (1) and (2) and taking natural log on both sides gives:

$$\ln(k) = \tau \frac{\Delta V^*}{k_B T} + \left(ln(A) - \frac{E_a}{k_B T}\right) \tag{3}$$

Therefore, on a semi-log plot of the reaction rate constant against the shear stress, the slope can be used to estimate ΔV^*.

1.2 Effect of Stress in Mechanochemical Activation

The effect of stress has been studied using the stress-augmented thermal activation model, i.e., the Bell model,[11] for many different processes, including wear, polymerization, and decomposition. Using this theory, wear of diamond-nanoparticle-containing amorphous carbon films sliding against Al_2O_3 was shown to be stress-induced since the wear rate increased exponentially with contact pressure.[12] A study on dimethyl-disulfide in a sliding

copper-copper interface showed that material growth in the form of polymers happened with negligible interfacial temperature rise, which indicated that the reactions leading to polymer formation were stress-induced.[13] Single-asperity measurement of the decomposition of methyl thiolate under compression on Cu surface showed that the reaction rate increased exponentially with normal stress.[14]

The ability of stress to activate a chemical reaction depends not only on the magnitude of the stress but also direction in which it is applied relative to the reaction coordinate. In fact, mechanochemical activation of molecules can require a very specific stress condition at a molecular level. For example, spiropyran, a common mechanochromic mechanophore, can be mechanically activated only if the applied force stretches the C-O bond, which is known to be the weak link of the mechanophore.[15] Other chemical systems have been shown to respond similarly to tensile stress that activates the reaction by elongating the mechanophore.[8] Such studies have demonstrated that the effectiveness of mechanical activation can vary dramatically based on the direction of stress, which can broadly be classified into either normal stress or shear stress.

1.2.1 Normal Stress Activation

Mechanochemical activation can be achieved without heat by applying normal stress. Such normal stress can be either compressive or tensile and applied to reactant molecules through methods including atomic force microscopy (AFM), optical tweezers, or ultrasonication.[16,17] Compressive stress has been shown to drive the mechanochemical decomposition of alkyl thiolate based mechanophores,[14,18] or to accelerate Diels-Alder reactions,[19,20] while tensile stress has been widely used to study the mechanochemical reactions in mechanophore-embedded polymers,[21,22] surface functionalization with single molecules,[6] and the unfolding mechanisms of proteins.[23–25]

1.2.2 Shear Stress Activation

Shear-activated or shear-driven mechanochemical reactions are usually carried out through grinding, milling, or rubbing motion[3,26–28] that transfers the mechanical energy of surfaces in relative motion to the reactant molecules. Shear-driven reactions dominate the chemistry at sliding interfaces in tribological systems.[9,10,29–31] Such reactions can lead to either material removal, i.e., wear at a tribological interface, or material accumulation. Material accumulation at a sliding interface can be formation of polymeric species through reactions of the interfacial molecules, or it can be protective film formation on the surfaces by the interfacial molecules. These protective layers, also known as tribofilms, are critically important for efficient function and durability of machine components because they reduce wear and friction. Shear stress can also play key roles in biochemistry. For example, shear stress can potentially drive or amplify the degradation of protein-based therapeutics.[32] However, the mechanisms underlying shear-driven reactions are not fully understood because of the complexity and dynamic nature of the interfacial conditions, which are continuously evolving during sliding.

1.3 Experimental Characterization of Shear-driven Reactions

1.3.1 Macroscale Experiments

Macroscale experiments have been used to understand the effect and contributions of shear stress on mechanochemical activation. Macroscale characterization has been largely

successful in demonstrating the effect of shear stress in tribofilm formation. For example, Ball-on-flat tribometer measurements of the tribofilm growth by zinc dialkyldithiophosphate (ZDDP) on tungsten carbide revealed that the film growth is driven mainly by shear stress rather than normal stress.[31] A similar dependance was also observed on steel surfaces.[33] A study on corrosion resistant phosphate coatings showed that tribofilms consisting of manganese phosphate formed on the uncoated counter-surface and the formation was shear induced.[34]

Polymerization reactions of simple organic molecules at a sliding interface in vapor phase lubrication (VPL) have been studied to explore how shear stress increases the reactivity of chemical species. Ball-on-flat experiments on allyl alcohol, α-pinene, pinane, and n-decane showed that polymerization was shear stress activated.[35–38] These experiments in VPL condition have also demonstrated the role of surface oxygen, ring strain, C=C double bond, and environmental water or oxygen molecules[39,40] in shear activation of mechanochemical reactions.

1.3.2 Nanoscale Experiments

AFM has been used for *in-situ* characterization of shear-driven reactions at the single-asperity scale. AFM-based experiments highlighted the role of stress-augmented thermal activation in tribofilm formation regardless of the presence of any catalyzer or involvement of any cation exchange.[29,41] AFM has been used to demonstrate the role of stress in material removal or wear. AFM combined with transmission electron microscopy was used as an in-situ technique to study the wear of silicon against diamond.[28] The wear of silicon was consistent with an atomic attrition mechanism where the rate of atom removal increased exponentially with contact stress. Another AFM-based study attempted to isolate the effect of lateral force on atom removal process. By investigating the rubbing-induced oxygen removal from graphene oxide using AFM, the study demonstrated the role of lateral forces generated by the velocity of the sliding tip in driving atomic scale wear. More generally, AFM is useful to image and measure reaction products. AFM has been used to measure the polymerization reaction yield from shear-driven reactions in ball-on-flat experiments.[35–38]

Although AFM is a powerful tool to investigate the role of stress in mechanochemical systems and to characterize reaction yield, decoupling shear stress and normal stress in AFM experiments is inherently difficult. Further, the rubbing motion of the tip on a substrate in contact mode AFM can cause a local rise in temperature which cannot be measured directly. Finally, even with the possible atomic scale resolution, AFM cannot capture *in*-situ atomic scale details of the shear-driven reactions, and thus, AFM experiments have not been able to demonstrate the molecular mechanisms of shear stress activation of chemical species.

1.4 Computational Modelling of Shear-Activated Reactions

Although experiments at different length scales have contributed to the understanding of shear-driven mechanochemical processes, these techniques cannot directly provide the in-situ stress state of the reactant species nor the reaction pathways with atomic resolution. Therefore, such experiments are often complemented by computational methods that can be used to elucidate experimental findings or to test different hypotheses. The use of computational methods, such as first principles calculations and molecular dynamics (MD)

simulations, can provide information about reactions between two surfaces that is not accessible in experiments.

1.4.1 First Principles-based Calculations

First principles calculations can accurately capture the atomic behavior of a system, and thus, quantum mechanics/molecular mechanics (QM/MM) simulations, ab initio calculations, and density functional theory (DFT) calculations have been used extensively to study shear-driven reactions such as tribofilm formation. Most of such computational works focused on the mechanisms and energetics of shear-driven reactions. QM/MM dynamic simulations were used to evaluate different dissociation mechanisms of molybdenum dithiocarbamates molecule at an Fe interface.[42] The study showed how oxygen atoms in the ligand position of the additive molecule and the metallic interface could alter the dissociation mechanism. Ab initio calculations identified the reaction pathway and associated energy barrier for adsorption of trimethyl-phosphite on Fe(110), and suggested that dissociative adsorption was energetically more favorable than molecular adsorption.[43] A subsequent first principles-based study showed that, at lower loads, the longer hydrocarbon chains tributyl phosphite could keep the surfaces farther apart than trimethyl phosphite.[44] DFT was used to calculate the activation energy for stress-assisted decomposition of methyl thiolate adsorbed on Cu(100) surface consistent with the experimentally calculated activation energies following the Bell model.[14] Another DFT study investigated three different reaction mechanisms of tricresyl phosphate decomposition on Fe(110) surface and showed that all three mechanisms could be thermally accessible.[45] DFT was used to develop a set of theoretical rules that successfully predicted the chemical behavior of several diatomic molecules when the molecules were stretched by an external mechanical force.[46] DFT-calculated reaction energy of siloxane bond formation at a silanol terminated silica interface suggested that the elastic deformation of the near-surface bulk region surrounding the contact could make significant contributions to the mechanochemical response of the system.[47]

Generally, most first principles-based studies only considered one or a few molecules with restricted dynamics since the calculations are extremely computationally expensive. DFT calculations involve no dynamics at all, and thus, cannot be used to study the dynamic evolution of a system. Some of these limitations can be circumvented using MD simulations. The development of reactive force fields such as ReaxFF has allowed MD simulations to study the chemical reactions of a wide range of complex tribological systems.[48] ReaxFF was initially developed to study hydrocarbon reactivity but later extended to a wide array of systems, including mechanochemical reactions at tribological interfaces.[49]

1.4.2 Reactive Molecular Dynamics Simulations

ReaxFF-MD simulations have been used to study mechanochemical reactions of different organic molecules and substituents. Reactive MD simulations complementing experiments in VPL have provided valuable insight on how shear stress drives tribochemical reactions. ReaxFF-MD simulations of polymerization of allyl alcohol and α-pinene in VPL identified shear stress as the key driver of oligomerization reactions and suggested that the mechanochemical activation of the reacting species was caused by shear-induced physical deformation.[35,50,51] Reactive simulations also explained experimental observations of α-

pinene tribo-polymerization reactions in VPL on stainless steel and silica [37,38]. The simulations identified shear stress, rather than normal stress, as the key factor driving association reactions of α-pinene molecules. A comparable value of activation volume in the experiments and simulations confirmed the relevance of the simulation results.

Shear-driven tribofilm formation mechanisms have also been studied using ReaxFF MD. The effect of alkyl substituents on mechanochemical reactions of phosphate esters under shear was studied and it was found that esters with secondary alkyl substituents had much higher dissociation rates than primary substituents.[52] A study on di-tert-butyl disulfide, an extreme pressure additive, on Fe(100) surfaces showed the decomposition pathway of the additive and found that the reaction yield across a range of different temperatures could be described by the Bell model.[53,54] Reactive MD simulations of thermal decomposition of two TCP isomers on Fe_2O_3 and Fe_3O_4 surfaces detected cresol as the main decomposition product, as observed in corresponding experiments.[51] Further, consistent with the experiments, MD simulations demonstrated the relative reactivity of the two isomers and the two surfaces.

ReaxFF simulations have been used to study the effect of shear-induced reactions on mechanochemical wear. ReaxFF studies on material removal from silica or silicon surface with water as a lubricant showed that water could have competing effects on wear.[55] Specifically, water can provide oxygen to the silica surface to form Si-O-Si bonds, which facilitates wear,[56,57] but can also minimize contact between the sliding surfaces, which reduces wear mechanically.[58,59] As such, ReaxFF-MD simulations have been shown to be a powerful tool for atomistic investigation of mechanochemical reactions and to provide valuable insights into the molecular mechanisms of mechanical activation.

1.5 Knowledge Gap

The discussion above highlights the complex nature of shear-driven mechanochemical reactions. In most applied shear-driven processes, the reactant molecules are subject to heat, normal stress, and shear stress. However, despite the current progress, individual contributions of heat, normal stress, and shear stress in shear activation of molecules remain unclear. Further investigation is necessary to determine the effect of different stress and thermal conditions on the activation mechanism of the reactants and the reaction pathway.

Moreover, the effect of chemical features and structure of reactant molecules on their shear activation is not fully understood. Small changes in the reactant structure have been shown to have significant impact on the shear sensitivity of the reactant molecule. There are no theories or models proposed in the current literature that can predict the shear sensitivity of specific chemical features. Thus, systematic investigation of the shear activation of homologous series of molecules is required.

Finally, the relation between the rate constant of a shear-driven reaction and the applied shear stress is captured by the Bell model. The model quantifies the concept of increasing the rate constant of a reaction by providing mechanical energy (E_m) which effectively lowers the overall activation energy. However, the mechanical energy term, E_m, is not fully understood. This is, in part, because its magnitude is coupled with the magnitude of E_a, e.g., a reaction with higher thermal activation energy will require more mechanical energy

to proceed. Also, mechanochemical reactions can follow completely different reaction pathways than their thermally driven counterparts[24,50] rendering the relation between E_a and E_m more complex. Importantly, the Bell model provides no information about the mechanism through which mechanical energy can activate a reaction.[60,61] Thus, uncovering the molecular mechanisms of shear activation requires further investigation.

1.6 Dissertation Outline

First, α-pinene ($C_{10}H_{16}$) molecules on silica surfaces were studied using reactive MD simulations at different interfacial conditions to identify the effects of heat as well as normal and shear stress on oligomerization reactions. This study focused on α-pinene because previous experimental work showed oligomerization of α-pinene could be stress assisted.[36–38] However, it was not clear if such oligomers can form thermally and, if so, how the thermal and shear-driven reaction pathways differ. To answer these questions, we performed heating simulations, compression simulations, and sliding simulations of α-pinene molecules at a silica-silica interface and studied the chemical reactions, including the reaction pathways, in the interface.

Next, mechanochemical reactions of a homologous series of simple cyclic organic compounds were studied using ReaxFF-MD to explore the effect of molecular structure on the susceptibility to mechanical activation. Previous studies of α-pinene, pinane, and n-decane highlighted the role of ring strain and C=C double bonds in shear-driven reactions.[37,38,50] Based on this, we modeled methylcyclopentane, cyclohexane, and cyclohexene on silica to investigate the mechanochemical response of a ring structure, double bond, and methyl side group in cyclic compounds. In the simulations, these precursors were subjected to normal and shear stress, and the resulting oxidative chemisorption and oligomerization reactions were tracked. Trends were compared to polymerization yield from ball-on-flat sliding experiments. Finally, the simulations were used to identify and compare oligomerization reaction pathways for the three molecules.

Finally, we focused on the shear-driven reactions of cyclohexene to investigate the role of molecular deformation in shear activation of reactants. Cyclohexene molecules were compressed and sheared between silica slabs in reactive MD simulations to induce oligomerization reactions. Trends in reaction yield and product from simulations were compared to ball-on-flat experimental results. Finally, deformation of the reactant molecules was closely analyzed to demonstrate a quantitative relationship between molecular deformation and reduction in energy barrier as predicted by the Bell model.

2 Reactive Molecular Dynamics Simulations of Thermal and Shear-driven Oligomerization

2.1 Introduction

Mechanochemical activation can require a very specific direction of stress at the molecular level such as compressive stress to drive the mechanochemical decomposition of alkyl thiolate based mechanophores,[14,18] or tensile stress to mechanochemically activate polymers embedded with spiropyran.[21,22] For shear-driven reactions, the *in*-situ stress state of the reactant molecules can be complex since most shear-driven processes happen at the interface of two sliding contacts where the reacting species are subject to heat, normal stress, and shear stress. Although the shear stress is expected to play the key role in shear-driven processes, other drivers can affect the reaction mechanisms and pathway. For example, experimental techniques at different length scales and computational modelling demonstrated the key role of shear stress in driving the protective film formation reactions by ZDDP and TCP molecules.[29,31,33,62] However, compressive stress has been shown to hinder the film growth in the case of ZDDP.[30] Identifying the individual role of all possible driving forces behind shear-driven reactions is crucial in developing a full understanding of shear activation.

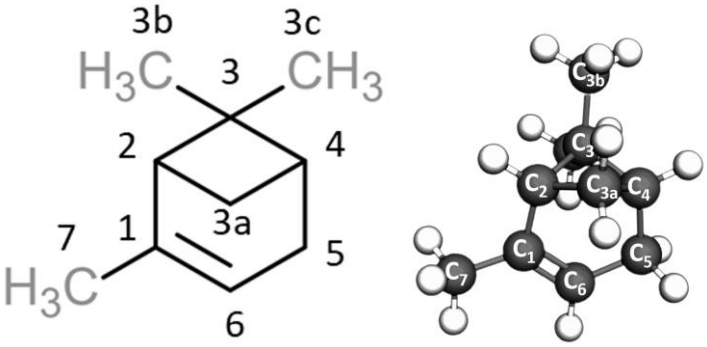

Figure 2.1: Structural formula and isometric view of the precursor molecule, α-pinene. The carbon atoms were numbered from one through seven according to the IUPAC convention. The four membered ring consists of C2, C3, C3a, and C4. The six membered ring consists of C1, C2, C3, C4, C5, and C6. The black and white atoms represent carbon and hydrogen, respectively.

In this work, α-pinene ($C_{10}H_{16}$) molecules on silica surfaces were studied using reactive MD simulation at different interfacial conditions to identify the effects of normal and shear stress, and heat on the oligomerization reaction. α-pinene is a 10-carbon bicyclic organic molecule with an interesting structure (Figure 2.1). The four membered ring of the molecule is highly strained due to the non-ideal bond angles, while the six membered ring of the molecule contains a C=C double bond. Thus, α-pinene allows the study of the effect of ring strain and C=C double bond on mechanochemical activation.

α-pinene has been previously used to study polymerization reactions in both ball-on-flat tribometer experiments and in simulations. Such studies showed that α-pinene polymerization under sliding conditions is mainly shear-driven and these reactions are promoted in oxidizing environments.[37,39] Oligomerization reactions of α-pinene were investigated in reactive MD simulations which showed that deformation of the four-membered ring triggered oligomerization.[38] However, individual contribution of heat, normal stress, and shear stress on α-pinene oligomerization is still not explicit. Further, a detailed comparison between thermal and shear-driven oligomerization reaction pathway will demonstrate clear distinctions between thermal and mechanochemical activation. Thus, in this work, we performed heating simulations, compression simulations, and sliding simulations of α-pinene molecules at a silica-silica interface. The simulation results identified shear stress as the key driver behind oligomerization of α-pinene molecules. Further, three oligomerization reaction pathways were observed under the identical shear condition, and how heat or shear activated each reaction pathway was investigated.

2.2 Methods

MD simulations of α-pinene molecules between two amorphous silica slabs (Figure 2.2) were carried out using the ReaxFF force field[48] with a set of parameters previously developed[63] from a combination of parameters for C/H/O[64,65], and Si/C interactions[66]. This force field was used for a similar system in a previous study[38]. All MD simulations were performed using the Large Atomic/Molecular Massively Parallel Simulation (LAMMPS) software[67]. Postprocessing was carried out using in-house python scripts and OVITO software[68].Figure 2.2

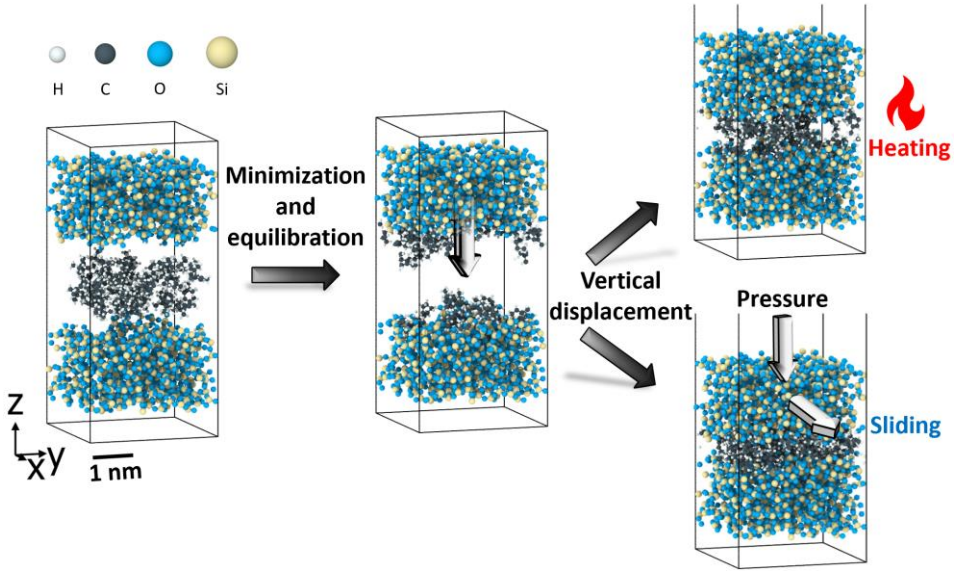

Figure 2.2: The simulation model system consisting of precursor molecules between amorphous silica slabs. From left to right: system equilibration (energy minimization and vertical displacement of the upper slab), and production simulations with heating or sliding. Production simulation for compression is not shown here. The white, black, blue, and yellow spheres represent H, C, O, and Si atoms respectively.

The amorphous silica slabs were created by a process that involved heating up crystalline cristobalite from 300 K to 4000 K at 0.02 K/fs and then cooling it down to room temperature at 0.02 K/fs cooling rate[38]. The presence of a vacuum on top of the slab during the annealing process produced a rough surface (~2 nm roughness) on each slab. The surfaces were then hydroxylated by introducing water molecules at 500 K. The final amorphous slabs were about 18.5 Å thick. Two such silica slabs were then positioned 22 Å apart, with 35 α-pinene molecules placed between the two slabs. The initial slab-to-slab distance was chosen to minimize interactions between the two slabs, provide enough space for the α-pinene molecules to equilibrate without mechanical stress, and minimize the computational time required to bring the slabs together. The number of α-pinene molecules was chosen to form at least a monolayer on each surface. The silica atoms 13.5 Å or farther from the two surfaces were treated as rigid bodies. The canonical ensemble (NVT) was applied to all other non-rigid atoms. Charge equilibration was performed throughout the simulation. The simulation timestep was 0.25 fs. The initial simulation box dimensions were 32.8 x 31.9 x 71 $Å^3$ with periodic boundary conditions in the x and y directions and fixed boundaries in the z direction.

Each MD simulation started with energy minimization and dynamic equilibration at 300 K. The upper slab was then moved towards the bottom slab in the z-direction until the two slabs were approximately 10 Å apart. After this point, the simulations were divided into three categories: heating simulations, compression simulations, and sliding simulations. For the heating simulations, the two slabs were held fixed at their position and the system was heated from 300 K to 900 K, 1200 K, or 1500 K at 1 K/ps heating rate followed by a 2 ns constant temperature simulation (Figure 2.2). The maximum normal stress experienced by the α-pinene molecules in the heating simulations was 0.45 GPa (tensile). For the compression simulations, the slabs were brought together at 300 K until the normal stress reached 1 GPa and the normal stress was maintained at this value for 500 ps. Then the system was subjected to a series of loading and unloading cycles for 2 ns. Each loading cycle involved the application of 1 GPa to the upper slab followed by an unloading cycle where the stress was relieved by lifting the upper slab and holding it 20 Å away from the lower slab. Finally, the effect of shear stress was studied in sliding simulations, where the upper slab was slid against the lower slab at 10 ms^{-1} sliding speed in the x-direction for 2 ns at 1, 2, 3, or 4 GPa compressive normal stress (Figure 2.2).

2.3 Results and Discussion

Oxidation of α-pinene at one or more carbon sites by surface oxygen atoms resulted in chemisorption of the molecules to the surface. The number of such oxidized molecules increased with time in all simulations (blue lines in Figure 2.3, Figure A1). At room temperature and without any mechanical stress, fewer than four of the 35 α-pinene molecules were oxidized. Then, either heat or mechanical stress was necessary to drive additional oxidation reactions. When temperature was increased to either 900, 1200, or 1500 K, without any stress, oxidation increased and then reached steady state where the system was at dynamic equilibrium. The number of oxidized molecules at dynamic equilibrium increased with temperature (Figure 2.3a, and Figure A1a and b).

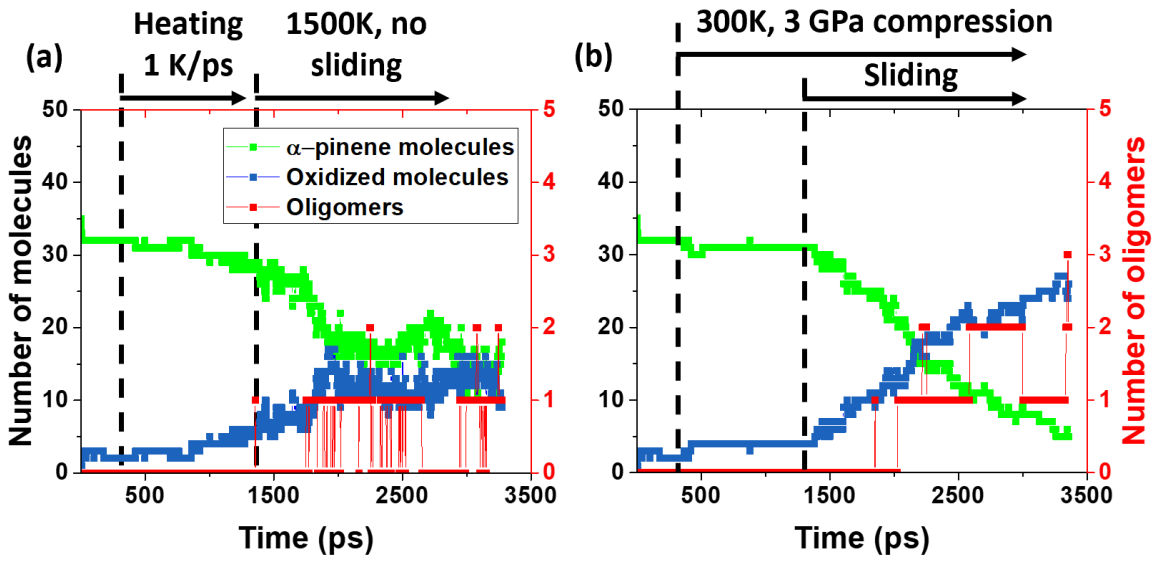

Figure 2.3: Evolution of chemical species in simulations at (a) 1500 K without pressure or sliding and (b) room temperature with sliding at 3 GPa. The number of α-pinene and oxidized molecules are plotted in green and blue, respectively, against the left ordinate axis and the number of oligomers is plotted in red against the right ordinate axis.

The effect of normal stress was tested with simulations at room temperature by moving the top slab downwards to apply 1 GPa contact pressure and then lifting it back up to release the pressure in cycles. It was found that, even after four cycles of loading and unloading, only two additional α-pinene molecules were oxidized (Figure A1c). This indicated normal stress could not efficiently drive these oxidation reactions. However, in sliding simulations, oxidation of α-pinene via reactions with the surface was observed at room temperature under all normal stress conditions. Representative results are shown for 1 GPa (Figure A1d) and 3 GPa (Figure 2.3b). The average shear stresses, calculated from the average friction force on the upper slab and the surface area, increased with applied normal stress (Figure 2.4). Of all the simulation conditions tested, the most oxidized molecules were observed in the sliding cases (Figure 2.3b, Figure A1d), suggesting shear stress plays an important role in α-pinene reactivity.

The number of α-pinene molecules after sliding started at each normal stress was fitted to the first order kinetics equation to calculate reaction rate (Figure A2). The reaction rates were then used to calculate activation volume from the slope of the linear relationship between the natural log of reaction rate and shear stress derived from the Bell model[11] using Equation (3). The calculated activation volume was 4.0±0.3 Å^3 (Figure 2.5), which is comparable to previously reported activation volumes for α-pinene (4.2-14.5 Å^3).[38,60]

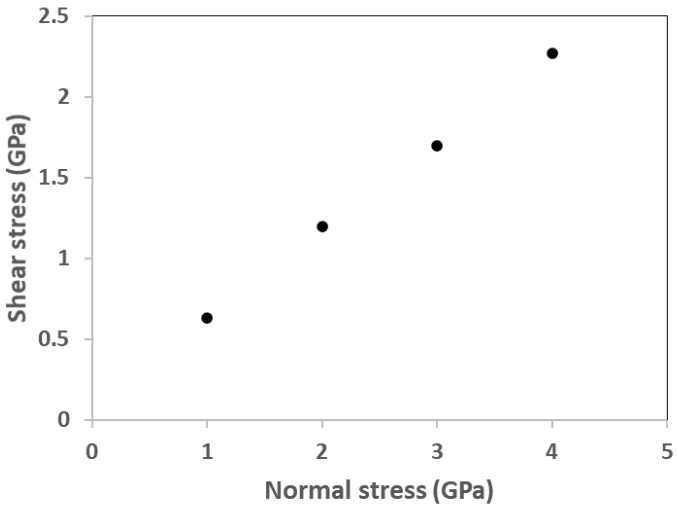

Figure 2.4: Average shear stress vs. applied normal stress in the sliding simulations. Shear stress was calculated from the lateral force on the upper slab and the surface area.

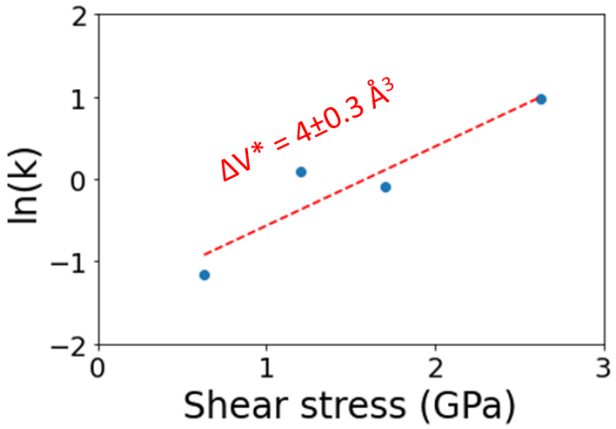

Figure 2.5: Calculation of the activation volume from the slope of a semi-log plot of the reaction rate constant vs. the shear stress, per Equation (3).

α-pinene is a bicyclic molecule consisting of the highly strained reactive four-membered ring (C2, C3, C3a, and C4) and the six-membered ring that contains the reactive double bond site (C1=C6), see inset to Figure 2.6a. The most reactive site on the α-pinene molecule for oxidative chemisorption was identified in each simulation based on the number of oxidation events. An oxidation event was counted for the first time when a covalent bond formed between a given carbon atom and a surface oxygen atom. Then the percentage of oxidation events at each carbon site relative to the total number was calculated (Figure 2.6). Interestingly, different trends were observed from the analyses of simulations with heating and sliding.

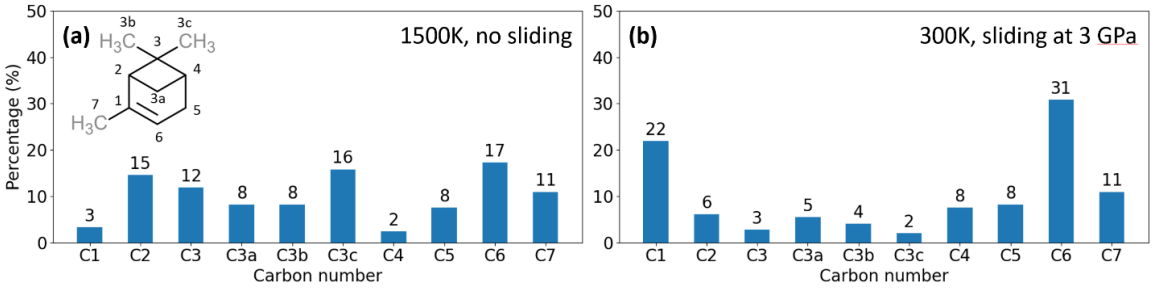

Figure 2.6: Percentage of oxidation at different carbon sites compared to all unique C-O bonds formed in simulations at (a) 1500 K without pressure or sliding and (b) room temperature with sliding at 3 GPa. At high temperature, carbon atoms in the four-membered ring were more reactive whereas, in the sliding simulation, carbon atoms at the double bond sites were more reactive.

At 1500K (Figure 2.6a), about 60% of the oxidation occurred at the four-membered ring (C2, C3, C3a, C3b, C3c, and C4) while only about 20% occurred at the double bond site (C1 and C6). The same trend was observed at 1200K (Figure A3b). At 900 K, both the four-membered ring and the double bond sites were oxidized equally (Figure A3a), but there were very few oxidized molecules (Figure A1), so the trend was not statistically significant. In the sliding simulations at 300 K, the double bond sites accounted for more than half of the total number of oxidized carbons while the four-membered ring was less reactive with fewer than 30% of the total oxidation (Figure 2.6b, Figure A3c). This indicated that shear stress enabled a reaction mechanism involving the double bond sites that differed from the thermal reaction pathway that involved reactions preferably at the four-membered ring.

Shear stress was also found to play a critical role in oligomerization of α-pinene molecules. Without sliding, oligomers only formed in simulations at 1500 K, the highest temperature tested (Figure 2.3, Figure A1), but not below 1200 K. The average thermal energy of 1200 K corresponds to 0.10 eV; no observation of oligomerization at this temperature means that the high-energy side tail of the Boltzmann distribution is still lower than or not comparable to the thermal activation barrier. In contrast, in sliding simulations, oligomers formed even at 300 K, indicating the barrier was reduced by shear to a level accessible by the high-energy tail of a Boltzmann distribution with an average thermal energy of 0.03 eV. Whether shear stress opened new reaction pathways for oligomerization or reduced the energy barrier for the same reaction pathway was investigated by studying the oligomerization reaction pathways.

Three oligomerization reaction pathways were found in the simulations, illustrated schematically and with snapshots from the simulations in Figure 2.7. Reaction pathway *A* started with oxidative chemisorption of an α-pinene molecule to the surface via one of its carbon atoms. Another α-pinene molecule, which could either be adsorbed to the surface or not, then reacted with the surface oxygen via the double bonded C6 atom in the six-membered ring. At that point, a dimer was formed through an ether linkage with the oxygen originally from the surface.

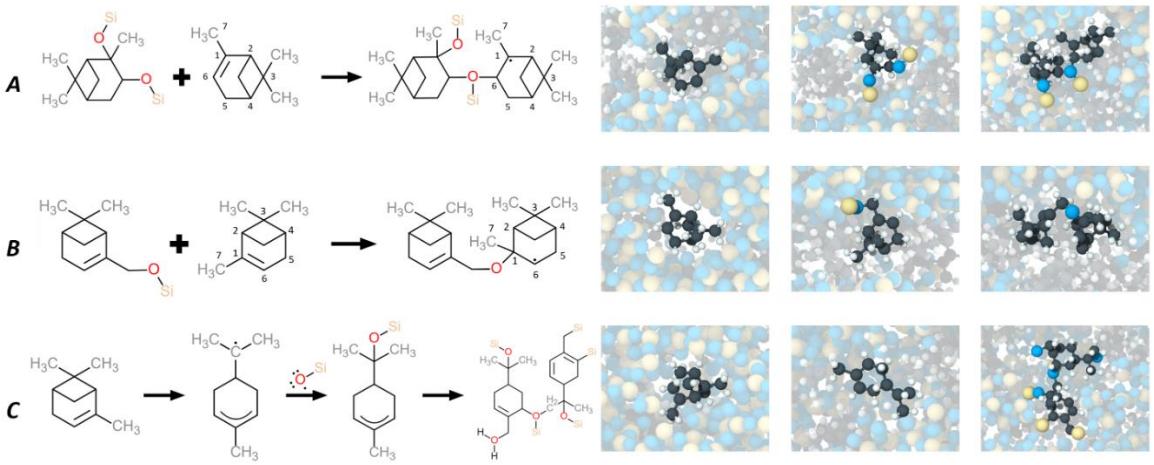

Figure 2.7: Representative oligomerization reaction pathways observed in the simulations illustrated schematically on the left and with corresponding snapshots from the simulations on the right. In the schematics, the atoms in the α-pinene molecules are numbered 1 through 6 based on IUPAC nomenclature while the methyl group at C1 is labeled C7 for convenience. In the snapshots, all atoms except those involved in the reaction are faded. Sphere colors are the same as those defined in Figure 2.2.

Reaction pathway *B* was initiated in a similar manner by oxidative adsorption of an α-pinene molecule by a surface oxygen atom. The oligomer was then formed when the surface oxygen reacted with the C1 atom of the double bond site of another α-pinene molecule. So, the double bond site (C1=C6) was activated in both pathways *A* and *B* to form a dimer through an ether linkage. However, in the first reaction pathway, C6 participated in forming the ether linkage whereas in the second reaction pathway, C1 was the participating atom.

Reaction pathway *C* started with opening of the four-membered ring by dissociation of one of the four C-C bonds in that ring. As the four-membered ring opened up, the entire α-pinene molecule was restructured to form an intermediate free radical molecule. This intermediate free radical was then oxidized by the surface. Two of such oxidized species finally reacted with each other to form an oligomer. Note that surface oxygen played a key role in all three reaction pathways. This suggests that environmental oxygen or water molecules may affect polymerization reaction rates, as observed experimentally.[39,40] The effects of oxygen-containing gaseous species on molecular mechanisms could be explored in future simulation-based studies.

Table 1 shows the number of oligomers formed in different simulations via the three reaction pathways. All 5 oligomers observed in the thermal simulation at 1500K were formed only through reaction pathway *C*; in contrast, 8 out of 9 oligomers observed in the sliding simulations were formed via pathways *A* and *B*. This suggests that only reaction pathway *C*, the reaction pathway that activated the four-membered ring (C2, C3, C3a, and C4), is accessible thermally. Shear, on the other hand, not only triggered the thermally accessible reaction pathway at a lower temperature, but also opened two new reaction pathways by activating a different reactive site, namely, the double bond site (C1=C6).

Such mechanochemical activation of α-pinene molecule was previously suggested to be the consequence of shear-induced molecular deformation.[38]

Table 1. Number of oligomers formed via the three reaction pathways in different simulations.

Reaction pathway	No sliding		Sliding	
	300K 1 GPa	900K – 1500K -	300K 1 GPa	300K 3 GPa
A	0	0	3	1
B	0	0	2	2
C	0	5	0	1

Deformation or structural change of a molecule can be identified just before covalent bond formation from the deviation in bond lengths and angles from their equilibrium values. Bond lengths and angles fluctuate about an equilibrium value and the amplitude and frequency of that fluctuation increase with temperature. The mode of a distribution of lengths or angles for multiple molecules at different times corresponds to the equilibrium value for a given molecular structure. Then, any persistent change in the length or angle due to distortion of the molecule would be reflected by a shift in the position of the mode or the formation of new peaks in the distribution. Previously, both length and angle histograms were used to investigate distortion of allyl alcohol molecules undergoing mechanically induced association reactions.[35]

Equilibrium carbon-carbon bond lengths and dihedral angles were calculated for all α-pinene molecules from simulations at 300 K and without any mechanical stress, shown as the black symbols/lines in Figure 2.8, Figure 2.9, Figure A4, Figure A5, and Figure A6. These equilibrium distributions were then compared with distributions for all non-oxidized reactants in reaction pathways *A* and *B* (Table 1) recorded at 50 different times during the 200 ps just before the ether linkage was formed.

In reaction pathway *A*, one reactant was anchored to the surface while the other reacted with its C6 atom to create the ether linkage (Figure 2.7). For the chemisorbed reactant, no consistent changes were observed in the bond length distributions indicating that no deformation occurred before oligomerization (data not shown). This could be explained by the fact that the dimerization reaction (ether linkage formation) occurs at the surface oxygen site to which the α-pinene molecule is anchored. However, the C1C2 and C4C5 bond lengths of the other reactant changed before the reaction, as evidenced by the shift of their respective bond length distributions to the left (Figure 2.8). For both bonds, there is a shoulder in the histogram at smaller distances indicating that the bonds were, on average, shorter. None of the other carbon-carbon bond lengths in the six-membered ring (Figure A4) or any dihedral angles (Figure A5) exhibited consistent deviations from their equilibrium values before the oligomerization reaction.

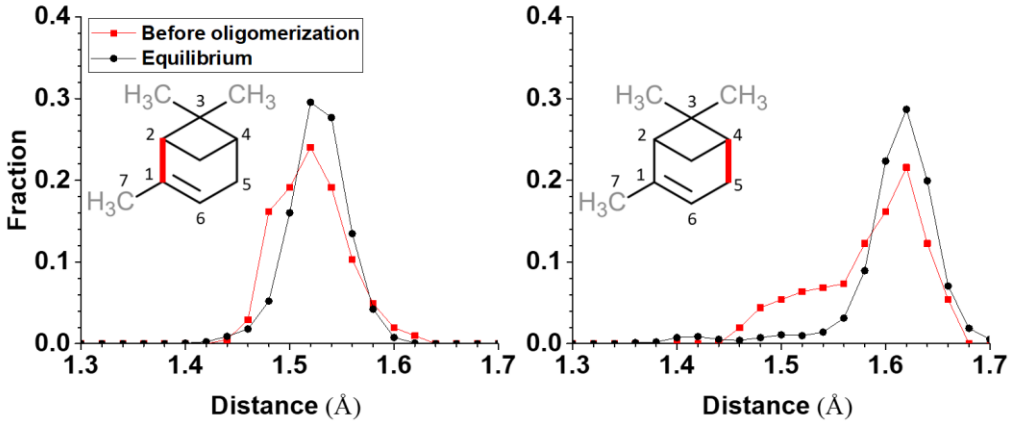

Figure 2.8: C1C2 (left) and C4C5 (right) bond length distributions at equilibrium (black) and before oligomerization through reaction pathway A (red). The red distributions were calculated over 200 ps before a dimeric species formed and averaged over four α-pinene molecules that were the non-oxidized reactants initially (i.e., reacting with the oxidatively chemisorbed species) in pathway A.

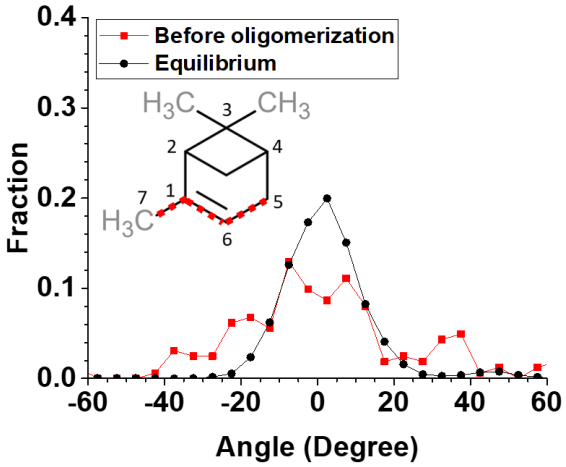

Figure 2.9: Comparison between C7C1C6C5 dihedral distributions at equilibrium (black) and before oligomerization through reaction pathway B (red). The red distribution was calculated over 200 ps before a dimeric species formed and averaged over four α-pinene molecules that were the non-oxidized reactant initially (i.e., reacting with the oxidatively chemisorbed species) in pathway B.

In reaction pathway *B*, one reactant was anchored to the surface while the other reacted with its C1 atom to create the ether linkage (Figure 2.7). Similar to reaction pathway *A*, the chemisorbed reactants did not show any consistent signs of deformation before oligomerization. However, the C7C1C6C5 dihedral angle distribution before oligomerization was distorted (Figure 2.9). Since C1 and C6 are sp^2 hybridized, at equilibrium, C7, C1, C6, and C5 should be in the same plane, making the equilibrium dihedral angle zero. Thus, any change in the dihedral angle suggests out of plane movement of C1 or C5 atom. However, the bond lengths in the six-membered ring closely followed their equilibrium values (Figure A6), which indicates that the C5 atom remained in plane

with C1 and C6. Thus, the distortion in the dihedral angle distribution can be attributed to the C7 atom. As the C7 moved out of the plane, it could in turn affect the hybridization state of the C1 atom, making it more reactive.

Distributions for reaction pathway *C* were not calculated since only a single oligomer formed via this pathway in the sliding simulations (Table 1). However, this reaction pathway was observed and analyzed previously where it was shown that the reaction was preceded by deformation of the four-membered ring.[38] Thus, for all three pathways, these analyses indicate that shear stress drives chemical reactions by deforming the molecular species to make them more reactive.

2.4 Conclusions

This work explored the contributions of heat and stress on mechanochemical association reactions forming tribofilms using a bicyclic molecule, α-pinene. At room temperature, both with and without normal stress, the reactivity of α-pinene molecules toward oligomerization was negligible. Reactivity increased with increasing temperature as more α-pinene molecules chemisorbed to the surface. Shear stress, on the other hand, could make the α-pinene molecules reactive even at room temperature and facilitated chemisorption. Analyzing the chemisorbed molecules showed that thermal activation facilitated reactions at the carbon atoms in the four-membered ring of the molecules, whereas shear activation opened reaction pathways at the double bond sites in the six-membered ring. Three oligomerization reaction pathways were found, all of which were readily accessible through shear, but rarely accessible thermally. Bond-by-bond analysis of the α-pinene molecules prior to oligomerization showed that shear caused structural deformation of the molecules from their equilibrium conformations. These results show clearly how heat and shear activate different chemical groups in α-pinene. However, the findings have more general implications for mechanochemical reactions.

First, the findings suggest a physical meaning for the activation volume in mechanochemistry.[60] The Bell model dictates that mechanochemical reactivity should increase exponentially with stress where the exponential stress dependence is related to an activation volume (ΔV^*) needed for the reaction to occur.[11] However, neither the magnitude nor the physical meaning of ΔV^* are fully understood.[60] Some studies compared it with the size of molecules involved in reactions or the unit cell of the substrate, while others suggested it reflects the degree of molecular deformation or deviation from the equilibrium structure.[60] The reactive MD simulation results of this study revealed shear induces reaction pathways that were not accessible in thermal reaction conditions (Table 1). The results also showed that the shear-induced pathways were made available through deformation of reacting molecular species from their equilibrium geometries (Figure 2.8 and Figure 2.9). This suggests that ΔV^* can be interpreted as the propensity of molecules to deform, supporting the hypothesis that activation volume is related to deformation. However, since this study included only one molecule, α-pinene, it cannot provide insight into a possible quantitative physical relationship between deformation and activation volume. Future studies with a homologous series of molecules subject to a range of shear stresses could reveal correlations between the degree of deformation (from the atomic trajectories) and the activation volume (determined from the shear stress dependence).

This study also has implications for reaction selectivity. It is known that, generally, mechanochemical reactions have lower selectivity than thermal reactions.[3,4] In thermal reaction conditions, the pathway with the lowest activation barrier (for example, pathway *C* for α-pinene shown in Figure 2.7) can be preferentially accessed by molecules in the high energy tail of the Boltzmann distribution.[69] In mechanochemical conditions, other pathways with higher thermal barriers are activated (as in pathways *A* and *B* in Figure 2.7). Depending on the molecular structure and reaction conditions, the lowest barrier pathway can vary. In fact, this is the primary strategy for controlling selectivity in most thermal reactions. In principle, the same should be possible if one knows how the reactant with a specific configuration is activated under what mechanical conditions. The reactive MD study presented here may open such opportunities.

Finally, this study demonstrates the use of reactive MD simulations as a tool for understanding how stress drives chemical reactions. Going forward, this simulation-based approach can be used to suggest ways to tune reactivity through molecular design or manipulation of operating conditions (stress and temperature) to achieve tailorable mechanochemical processes.

3 Shear-Activated Chemisorption and Association of Cyclic Organic Molecules

3.1 Introduction

The preliminary work on α-pinene showed how shear-driven reaction pathways can differ from thermal reactions pathways, and the role of shear-induced deformation in mechanochemical activation of molecules. These results not only offer intriguing insights into the atomistic details of mechanochemical reactions but also arouse further questions about the effect of other functional groups or chemical features of molecules on their mechanochemical activation. Further, recent studies on application relevant materials, such as ZDDP and phosphate esters have showed that the mechanochemical response of molecules can change depending on their chemical features, evident from the change in reaction rate, activation volume, or pre-exponential constant.[52,70,71] Thus, expanding this research to study the mechanochemical activation of other simple organic molecules with different chemical features is necessary.

In this work, we studied shear-activated reactions of simple cyclic organic molecules to isolate the effect of chemical structure on reaction yield and pathway. Reactive molecular dynamics simulations were used to model 50 methylcyclopentane, cyclohexane, or cyclohexene molecules subject to pressure and shear stress between silica surfaces. Tribochemical reactions in all three simulated systems were analyzed and the susceptibility to mechanochemical activation of the three precursor molecules was evaluated and compared.

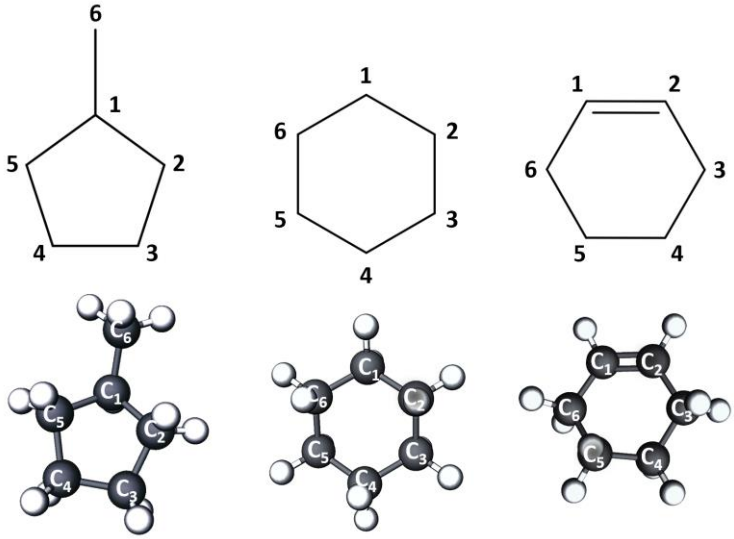

Figure 3.1: Structural formula and isometric view of the three precursor molecules, from left to right, methylcyclopentane, cyclohexane, and cyclohexene. The carbon atoms of the molecules were numbered from one through six according to the IUPAC convention. The color scheme of the atoms is the same as in Figure 2.2.

3.2 Methods

MD simulations of cyclohexane, cyclohexene, and methylcyclopentane precursors sheared between two silica surfaces were performed to study the molecular mechanisms of shear-induced reactions (Figure 3.2). QuantumATK[72] was used to create three model systems, each containing 50 molecules of one of the three precursors confined between two silica slabs. The number of precursor molecules was chosen to form at least one monolayer on each surface. The amorphous silica slabs were created using a heat and quench method that involved heating a cristobalite slab to 4000 K and then cooling it back to room temperature, with a heating and cooling rate of 0.02 K/fs.[38,50] The cristobalite was placed next to a vacuum region during the amorphization process to form a silica surface with 2 Å average roughness. The surfaces were then passivated by reacting them with water molecules until the number of reactions between the water and the surface reached steady state.

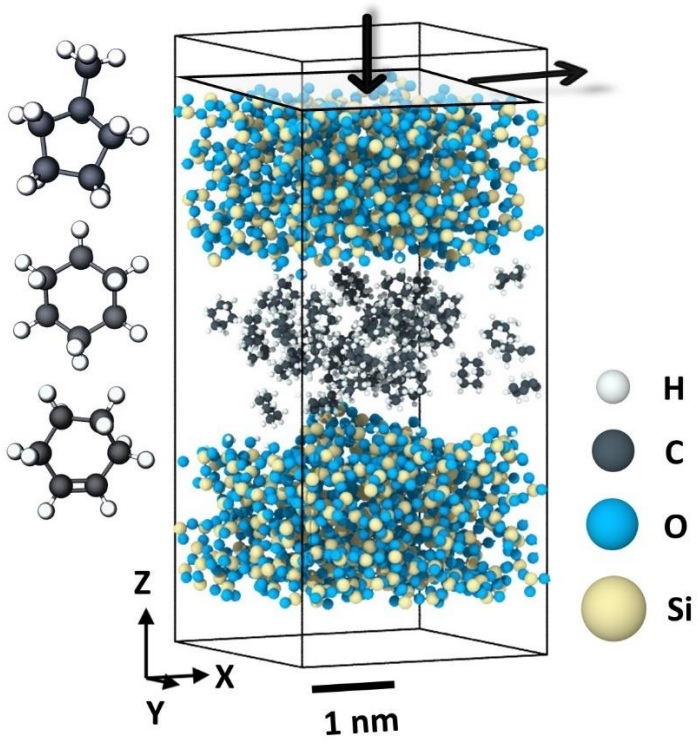

Figure 3.2: The model system consisting of methylcyclopentane, cyclohexane, or cyclohexene (shown individually on the left) confined and sheared between amorphous silica slabs. The white, black, blue, and yellow spheres represent H, C, O, and Si atoms, respectively.

The two silica slabs initially were placed 22 Å apart to minimize interactions between the slabs, provide enough space for the precursor molecules to equilibrate without mechanical stress, and minimize the computational time required to bring the slabs together. Any silica atoms 13.5 Å or farther from the two surfaces were treated as rigid bodies and all other atoms were treated as non-rigid, movable atoms. The initial simulation box dimensions were 33 x 32 x 71 $Å^3$ with periodic boundary conditions in the x- and y-directions and fixed boundaries in the z-direction.

Each MD simulation started with energy minimization and dynamic equilibration at 300 K. The upper slab was then moved towards the bottom slab in the z-direction until the average distance between the two slabs was approximately 10 Å. Then the system was compressed at 1, 3, or 4 GPa pressure for 250 ps by applying load on top of the upper slab. To increase the reactivity of the precursor molecules, the temperature of the system at 4 GPa pressure was increased to 450 K at 1 K/ps rate after the compression stage. Finally, sliding simulations were carried out by moving the upper slab at 10 ms^{-1} speed in the x-direction for 2 ns. The canonical ensemble (NVT) was applied to all non-rigid atoms and charge equilibration was performed throughout the simulation.

The interactions between atoms were modeled using the ReaxFF force field[48,63] with a set of parameters previously developed from a combination of parameters for C/H/O,[64,65] and Si/C interactions.[66] This force field was used for a similar system previously to study thermal and shear-driven oligomerization of α-pinene.[38,50] The time step for dynamics was 0.25 fs. All simulations were performed using the Large Atomic/Molecular Massively Parallel Simulation (LAMMPS) software.[67] Postprocessing was carried out using in-house python scripts and OVITO software.[68]

3.3 Results and Discussion

The initial reaction for all precursor molecules was oxidative chemisorption, resulting in a reduction in the number of intact precursor molecules in the system. Figure 3.3 shows this reduction in precursor molecules and corresponding increase in the oxidized chemical species. Without sliding (before 0.75 ns), only a few molecules reacted with surface oxygen at any temperature or pressure (Figure 3.3 and Figure A7). The increase in oxidative chemisorption coincided with the onset of sliding, demonstrating that shear stress accelerated oxidative chemisorption of all three precursors. Similar observations have been made for other simple organic molecules, including α-pinene and allyl alcohol, in both experiments and simulations.[35,38,39,50] Here, interesting observations can be made from the relative reactivity of the three precursors.

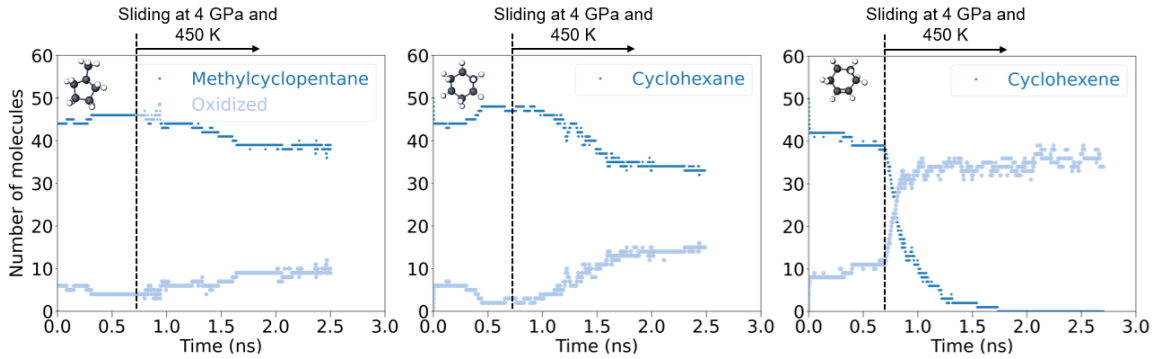

Figure 3.3: Evolution of the number of intact methylcyclopentane, cyclohexane, and cyclohexene molecules and corresponding change in the number of oxidized species in simulations at 4 GPa and 450 K. Sliding started from 0.75 ns, after the system was equilibrated, compressed to 4 GPa, and heated from 300 K to 450 K.

For methylcyclopentane and cyclohexane at 300 K, very little oxidative chemisorption was observed at any pressure condition tested (Figure A7). At 4 GPa and 450 K, the reactivity

of cyclohexane increased slightly relative to the 300 K cases, but there was no change in the reactivity of methylcyclopentane. At any temperature and pressure condition, cyclohexene produced the most oxidized species. For cyclohexene, the activation volume was calculated from the reaction rate constants at different pressures according to Equation (3) and found to be 5.6 ± 1.5 Å^3, which is comparable to the values reported for polymerization of similar chemical species in previous studies.[35,38,50] Activation volume could not be calculated for cyclohexane or methylcyclopentane due to their low reactivity.

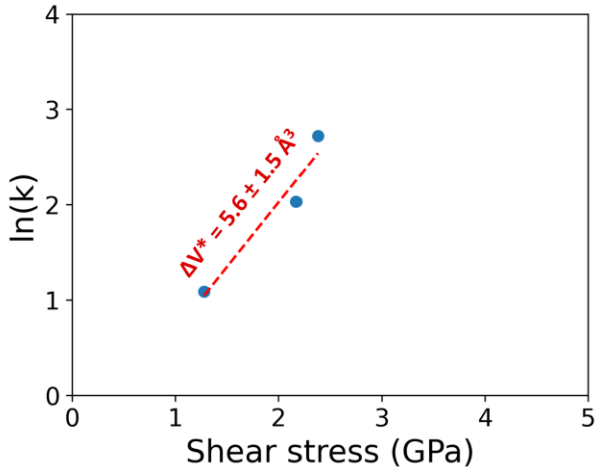

Figure 3.4: Calculation of the activation volume of cyclohexene from the slope of a semi-log plot of the reaction rate constant vs. the shear stress, per Equation (3) Shear stresses in the simulations were calculated from the friction force on the upper slab and the contact area.

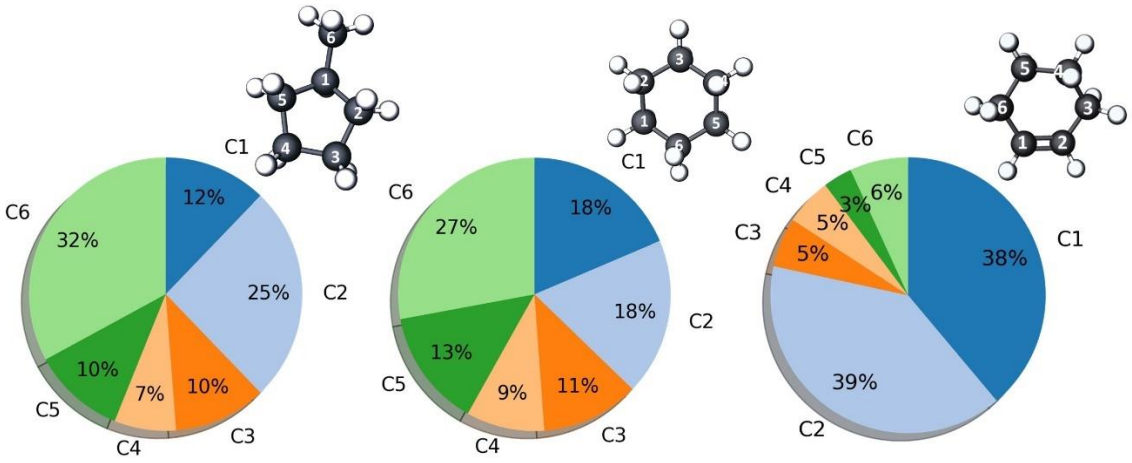

Figure 3.5: Probability of each carbon site on the three precursors participating in an oxidative chemisorption reaction. Data from all four pressure and temperature condition simulations was used in the analysis for each precursor.

The difference in the reactivity of the three compounds was further investigated by characterizing the oxidative chemisorption at each carbon. Methylcyclopentane, cyclohexane, and cyclohexene molecules have six potential carbon sites (C1-C6) at which

oxidative chemisorption reactions can occur. The most reactive site for oxidative chemisorption was identified by calculating the percentage of oxidation reactions that occurred at each carbon site with respect to the total number of oxidation reactions for a given precursor. An oxidation reaction was defined as formation of a covalent bond between a carbon atom and a surface oxygen atom. Data from simulations at all temperature and pressure conditions for each precursor was used for this analysis and the results are shown in Figure 3.5.

For methylcyclopentane, the C2, C5, and C6 carbon sites neighboring the tertiary C1 site accounted for 67% of all methylcyclopentane oxidation reactions, which suggests that these sites are more responsive to mechanochemical activation. Especially, the methyl side group (C6) was found to be the most reactive. Cyclohexane is a symmetrical molecule, so all six carbon atoms of the molecule should have relatively equal probability of participating in an oxidation reaction. However, the distribution in Figure 3.5 is not symmetric, likely due to the small number of total oxidation reactions observed in the cyclohexane simulations (Figure 3.3 and Figure A7). Finally, for cyclohexene, about 80% of all oxidation reactions happened at the double bond sites (C1 and C2), indicating that the C=C double bond is very susceptible to mechanochemical activation. The probabilities calculated for cyclohexene are statistically more significant than the other two precursors due to the much higher number of observed cases of cyclohexene oxidation reactions ((Figure 3.3 and Figure A7).

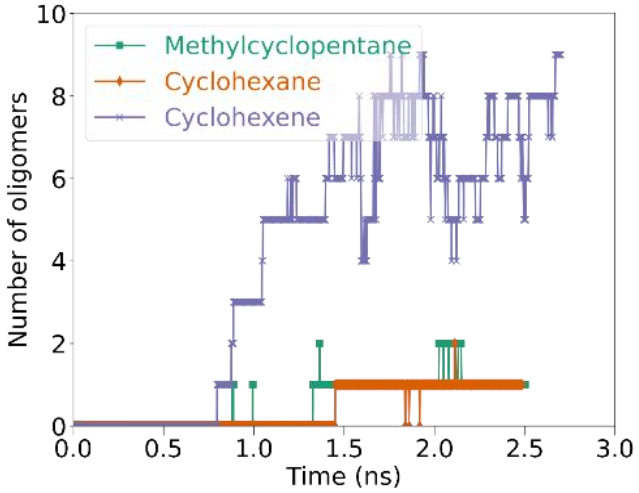

Figure 3.6: Number of oligomers in simulations of methylcyclopentane, cyclohexane, and cyclohexene at 4 GPa and 450 K. Sliding started at 0.75 ns.

Oxidative chemisorption has been shown previously to precede polymerization or oligomerization in both tribometer experiments and simulations.[35,37–39,50] Figure 3.6 shows the evolution of oligomers in the simulations for the three precursors at 4 GPa pressure and 450 K. For all three precursors, no oligomers formed before sliding started, which indicated that oligomerization of the molecules was mainly driven by shear stress. Fewer than three oligomers were detected for either methylcyclopentane or cyclohexane after sliding for 2 ns. In contrast, about eight oligomers formed during the same time for cyclohexene (Figure

3.6). The oligomerization trends are consistent with those observed for oxidation. This suggests that oxidation is the first step in the oligomerization reaction pathway, as observed previously for shear-driven association reactions of α-pinene.[50]

To confirm the trends observed in the simulations, experiments with similar conditions were carried out. Figure 3.7 shows AFM images of one end and the middle of the sliding tracks after 600 reciprocating sliding cycles. The line profiles of the middle of sliding track show more accumulation of reaction products for cyclohexene than the other two precursors. We estimated the amount of reaction product from the volume of material above the silica reference plane to be $(16.1\pm6.6)\times10^3$, $(8.7\pm2.9)\times10^3$, and $(45.9\pm5.8)\times10^3$ μm^3 in methylcyclopentane, cyclohexane, and cyclohexene, respectively. The experimental reaction products were polymeric species, and so not directly comparable to the results for dimers in the simulations. However, the much larger reaction product yield for cyclohexene in the experiments is qualitatively consistent with trends in the simulations (Figure 3.6). This indicates that the simulations reproduced the comparative reactivity of the three precursors during mechanochemical excitation.

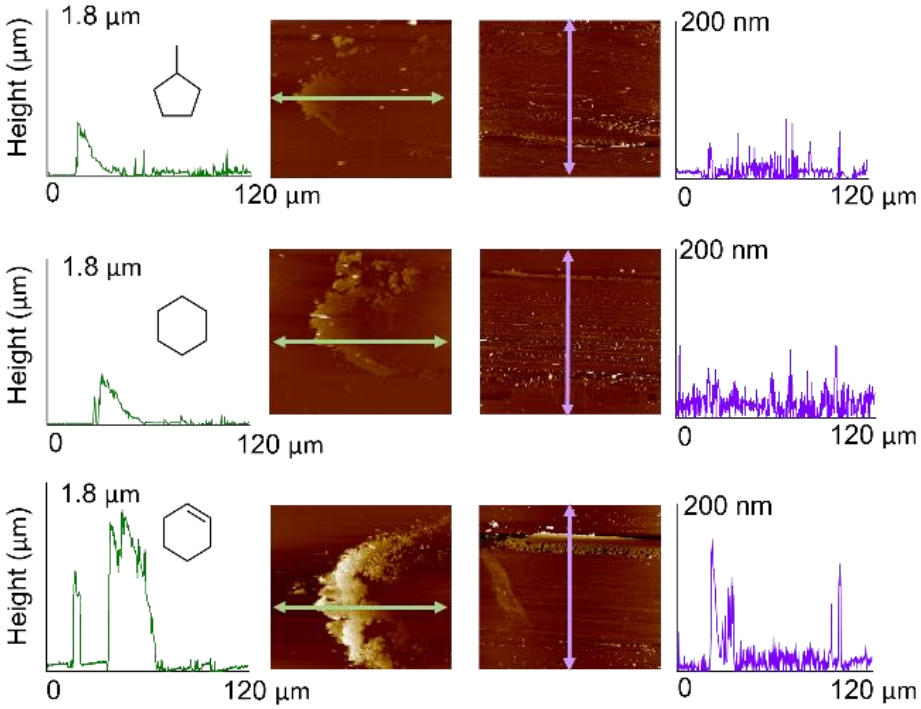

Figure 3.7: AFM images and the height profiles of the reaction products accumulated at the ends (left) and the middle (right) of the sliding track after the shear-induced mechanochemical reactions of methylcyclopentane, cyclohexane, and cyclohexene. The size of the images is 120 × 120 μm^2. The figure and all its contents were provided by Yu-Sheng Li and Dr. Seong H. Kim.

Next, the simulated oligomerization reaction pathways of all three precursors were investigated to identify the molecular mechanisms of mechanochemical activation. Figure 3.8 shows snapshots of the key steps of the oligomerization reaction pathways for methylcyclopentane, cyclohexane, and cyclohexene. Both methylcyclopentane and

cyclohexane followed a similar pathway, which began through hydrogen elimination of an intact precursor molecule. The hydrogen elimination reaction happened between a surface siloxane and a precursor molecule, eventually forming silanol and an undercoordinated carbon atom. These undercoordinated atoms are identified by red asterisks in Figure 3.8. In the case of methylcyclopentane, the carbon at the methyl group (C6) was the most reactive site for the hydrogen elimination, whereas all six carbon atoms of cyclohexane were equally likely to undergo hydrogen elimination. Next, the undercoordinated carbon atom reacted with another surface oxygen, identified by a small black circle in Figure 3.8, resulting oxidative chemisorption of the radical. This second step could happen through reaction with either a surface silanol or a siloxane group. Finally, a second hydrogen-deficient or oxidized precursor reacted with the first oxidized species to form an oligomer through an ether linkage.

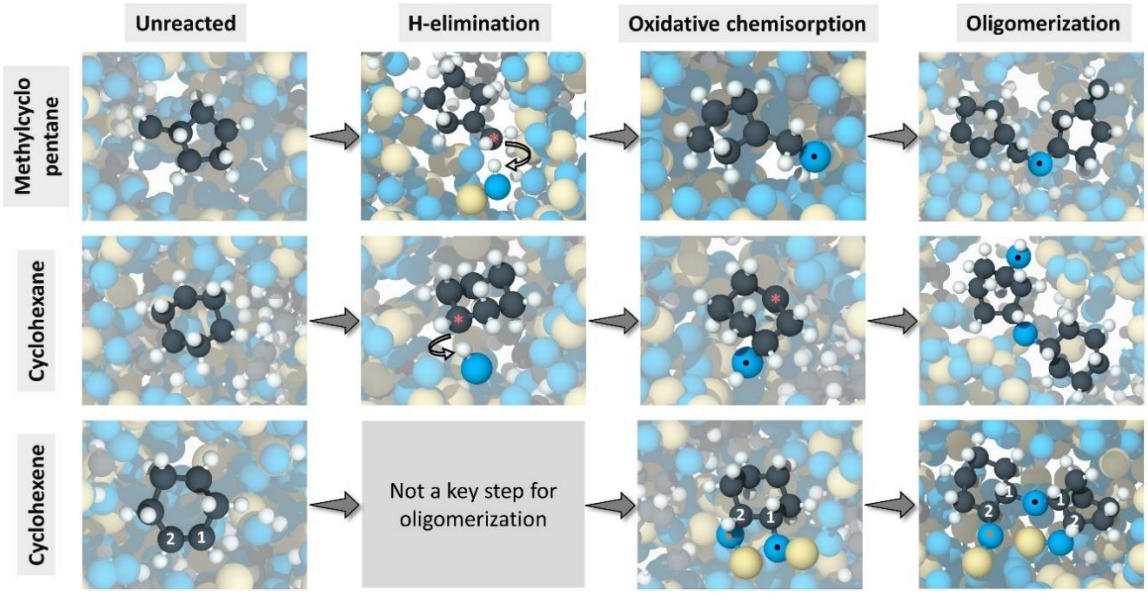

Figure 3.8: Simulation snapshots showing the key steps of the oligomerization reaction pathways for the three precursors. Although hydrogen elimination was a key step for oligomerization of methylcyclopentane and cyclohexane, all observed oligomerization reactions of cyclohexene involved direct oxidation at the double bond site (C1=C2). Undercoordinated C atoms are identified with a red '*' in the snapshots. Oxygen atoms shown in consecutive snapshots of a pathway are identified with a coloured dot. From left to right, the snapshots were taken approximately at simulation times of 0, 1.0, 1.3, and 1.6 ns for methylcyclopentane; 0, 1.1, 1.3, and 1.5 ns for cyclohexane; and 0, 0.7, and 0.9 ns for cyclohexene.

In contrast, cyclohexene followed a reaction pathway that involved direct activation of the double bond site to form oligomers. Cyclohexene oligomerization reactions started with oxidative chemisorption of an intact molecule at one or both double bond sites. This is shown in Figure 3.8 as carbon atoms labeled 1 and 2 bonding with oxygen atoms identified with small orange or black circles. Then, another intact or oxidized cyclohexene molecule reacted with the first reactant to form an ether linkage. This, in turn, resulted in the formation of an oligomer. Although cyclohexene could undergo hydrogen elimination

followed by oxidation like the two other precursors, no oligomer was observed to form through this pathway. Note that, since surface oxygen atoms played a crucial role in all oligomerization reactions, the presence of chemical species such as water or oxygen at the interface may affect the oligomerization reaction pathways,[39] although this could not be studied using the present model systems.

To investigate if the shear-driven reactions or reaction mechanisms described above could be driven thermally, simulations without applied normal or shear stress were run at 900 K for all three precursors. These simulations at 900 K will be referred to as heating simulations. The model systems for the heating simulations were the same as those used in the sliding simulations, described in the Methods section. The simulation protocol for the heating simulations was as follows: energy minimization and system equilibration at 300 K, moving the upper slab towards the bottom slab until the pressure at the interface reached ~0.5 GPa (tensile), fixing the positions of the slabs, ramping up the temperature to 900 K at 1 K/ps heating rate, and finally, production simulation at 900 K without applying any additional normal pressure or sliding motion.

Methylcylopentane and cyclohexane remained unreactive with no oxidative chemisorption observed (Figure A9). Cyclohexene exhibited some oxidation at 900 K, but the reaction rate was much lower than observed in the sliding simulations at room temperature at any normal stress. No oligomers were observed in any of the heating simulations, suggesting that the thermal energy needed for oligomerization was higher than the energy available at 900 K. Since no oligomers formed thermally, direct comparison between thermal and shear-driven reaction pathways could not be made. However, in previous study of α-pinene using a similar model system, oligomerization reaction pathways and reaction intermediates at temperatures above 900 K were found to differ from shear-activated pathways.[50]

3.4 Conclusions

In this work, mechanochemical activation of methylcyclopentane, cyclohexane, and cyclohexene molecules subject to compression and shear at a silica interface was studied using reactive MD simulations. The precursor molecules reacted with surface oxygen atoms to undergo oxidative chemisorption reactions that were mainly driven by shear stress. Methylcyclopentane and cyclohexane exhibited low responsiveness to mechanical activation since the yield of oxidative chemisorption for these precursors was quite low even at high pressure and elevated temperature. In contrast, cyclohexene was found to be very sensitive to mechanical activation, participating in many oxidative chemisorption reactions at all simulated pressure and temperature conditions. Analyzing the chemisorbed molecules revealed that the difference in the reactivity of the precursor molecules stemmed from the difference in their chemical features. In the case of methylcyclopentane, most of the oxidation reactions happened at the methyl group side of the molecule, whereas, for cyclohexene, about 80% of all oxidation reactions happened at the double bond sites. Oxidative chemisorption of the precursor molecules eventually led to oligomer formation and cyclohexene was observed to form the most oligomers at all pressure and temperature conditions. This trend was in qualitative agreement with the tribopolymer yield observed in ball-on-flat tribometer experiments. Analyzing the oligomerization reaction pathways showed that both methylcyclopentane and cyclohexane followed a similar mechanism of

hydrogen elimination followed by oxidation and, finally, oligomerization. Cyclohexene, however, did not require hydrogen elimination to form oligomers since direct oxidation at the double bond sites facilitated oligomerization. The results of this study show how chemical structure can change the mechanical activation mode and may also suggest ways to introduce chemical species as mechanophores in polymers or substituents in stress-activated reactants to tune reactivity.

4 Shear-Activation of Mechanochemical Reactions Through Molecular Deformation

4.1 Introduction

The previous study on the shear activation of α-pinene captured quantifiable signs of molecular deformation prior to shear-driven reactions occurred. In fact, it has been proposed that the mechanism underlying mechanical activation is deformation of reactants from their thermally and chemically stable conformation.[36,60] Macroscale experiments have shown a connection between mechanochemical activation and physical deformation of material by measuring applied strain. For example, the mechanochemical response of a dimeric anthracene-based mechanophore was investigated by compressing a mechanophore-embedded composite, revealing that the mechanophores exhibited activation upon deformation beyond a critical strain threshold.[73] Similar observations were made for the mechanochromic response of spiropyran-linked elastomers under compression and tension tests, demonstrating that a threshold strain was essential to initiate the mechanochemical reaction.[15] Such critical or threshold strain observed in macroscale experiments suggested that mechanochemical activation was triggered by physical deformation of mechanophores. Stress-induced deformation has been investigated at the molecular level by measuring change in molecular length under tension. AFM studies conducted with proteins and mechanochromic mechanophores showed that stretching the mechanophore molecules changed their length and molecular structure, eventually reshaping the potential energy surface of a reaction.[17,24,25,74,75] Surface functionalization with a single molecule was achieved by first attaching a polymer to the surface using AFM and then stretching the polymer chain between the tip and the surface to cause a chain dissociation, leaving the desired chemical species on the surface without the need for additional reactants or catalysts.[6] Such extension in polymer length has been shown to deform bond lengths and angles in the polymer backbone.[76,77] AFM experiments on the mechanochemical decomposition of methyl thiolate molecules revealed that the decomposition reactions could not be driven effectively below a critical stress threshold required for the reactant molecules to buckle.[18] However, directly observing molecular deformation is challenging with experiments, so they are often complemented by computational tools.

Quantum chemistry-based calculations using an extreme pressure polarizable continuum model showed molecular deformation during mechanochemical activation under hydrostatic stress by calculating the change in the volume of the van der Waals cavity of reactant molecules.[78,79] Density functional theory (DFT) calculations showed how molecular structure could be affected by mechanical stress during pericyclic reactions. Specifically, cyclobutene and benzocyclobutene under mechanical stress were found to undergo thermally forbidden electrocyclic ring opening reactions.[16,80] Such reactions could not be explained by the typical pericyclic selection rule since the electronic structure of the reactant under mechanochemically distorted reaction pathway remained similar to the electronic structure in thermal pathway.[81] DFT calculations also revealed that the optimized structure of reactant molecule under mechanical stress deviated from the fully

relaxed molecule and that mechanical stress could modify the potential energy surface by deforming C-C bonds.[80,82] DFT-calculated reaction trajectories for [4+2] Diels-Alder cycloadditions between anthracene and dienophiles showed that the reaction energy barrier decreased with increasing distortion of the anthracene C-C-H angle.[20] Although first-principles or DFT-based calculations provide accurate description of the reactant structure and energies associated with mechanochemical reactions, such calculations are extremely computationally expensive, limited to small system size consisting of few atoms, and have no or limited dynamics.

Most of the drawbacks associated with first-principles or DFT calculations can be circumvented, albeit at the expense of some accuracy, using reactive molecular dynamics (MD) simulations.[49] Reactive MD simulations of a dimeric 9-anthracene carboxylic acid (Di-AC) mechanophore-embedded polymer showed that the critical strain required for mechanochemical activation was related to the elongation of a C-C bond.[73] Reactive MD simulations of the [4+2] Diels-Alder cycloadditions between anthracene and dienophiles showed that increasing compressive stress induced more distortion of the anthracene C-C-H angles before the reaction occured.[20] A hybrid MD simulation framework integrating a classical force field and ReaxFF captured the physical entanglement between an epoxy network and a cyclobutane-based mechanophore embedded polymer chain, and showed that the intensity of fluorescence was directly proportional to the deformation of the mechanophore.[83] Another study on dimeric anthracene-based mechanophore using the same hybrid MD simulation framework predicted the critical strain for the activation of the mechanophore embedded polymer that was in good agreement with experimental findings.[73] Reactive MD simulations have also been used to investigate molecular deformation in shear-driven reactions. Reactive MD simulations complementing ball-on-flat tribometer experiments captured significant distortion of C-C bonds lengths in allyl alcohol[35] and α-pinene[38,50] molecules prior to shear-driven oligomerization reactions. Despite this progress, a clear connection between molecular deformation and mechanical energy is missing, especially for shear-driven reactions where the *in situ* stress and energy states are complex.

Our previous research on cyclohexene explored shear-driven oligomerization reactions on stainless steel in inert, oxidizing, and reducing environments, and on hydroxylated silica in inert environment.[84,85] These studies showed easier mechanochemical activation during sliding for cyclohexene than for similar molecules such as cyclohexane and methylcyclopentane on both stainless steel and hydroxylated silica. Complementary reactive MD simulations revealed the shear-driven reaction pathways and identified the C=C double bond of the cyclohexene molecule as the source of its shear sensitivity.[84] However, the role of molecular deformation in mechanochemical activation within the context of the Bell model was not explored.

Therefore, this work aims to understand the effect of molecular deformation on the energetics of shear-driven mechanochemical reaction. Specifically, mechanochemical oligomerization of cyclohexene molecules is studied using reactive MD simulations, complemented by ball-on-flat tribometer experiments in a vapor phase lubrication (VPL) condition, to investigate the shear activation of chemical reactions. Experiments confirm polymerization reactions are driven by shear stress and provided information about the products and pressure-dependence of the reaction. The simulations show similar trends and

are analyzed with specific focus on identifying and quantifying shear-induced deformation. Finally, nudged elastic band (NEB) calculations are used to calculate the energy barrier for oligomerization reactions with undeformed or deformed reactants and the trends are analyzed to identify a relationship between the mechanical energy term in the Bell model and molecular deformation.

4.2 Methods

4.2.1 Simulation Methods

MD simulations of cyclohexene molecules sheared between two silica slabs were conducted using the Large Atomic/Molecular Massively Parallel Simulation (LAMMPS) software.[67] The timestep was 0.25 fs. The interactions between atoms in the simulations were modeled using the ReaxFF force field[48] with a set of parameters previously developed[63] from a combination of parameters for C/H/O[64,65] and Si/C[66] interactions. The forcefield used here[51] was reparametrized based on the three source forcefields[52-54] to model uniaxial tension and compression of solid polytetrafluoroethylene and liquid polydimethylsiloxane polymers. The reparameterization process involved direct comparison of ReaxFF model predictions to DFT calculations. For example, the C-C, C-H, and C-O bond compression/extension energies were compared with corresponding DFT calculations during the reparameterization process until satisfactory agreement was achieved.[51] This force field has been used to study mechanochemical reactions in similar systems, specifically the shear-driven oligomerization of α-pinene,[38,50] cyclohexane, methylcyclopentane, and cyclohexene.[84,85] Postprocessing of the simulation data was carried out using in-house python scripts and OVITO software.[68]

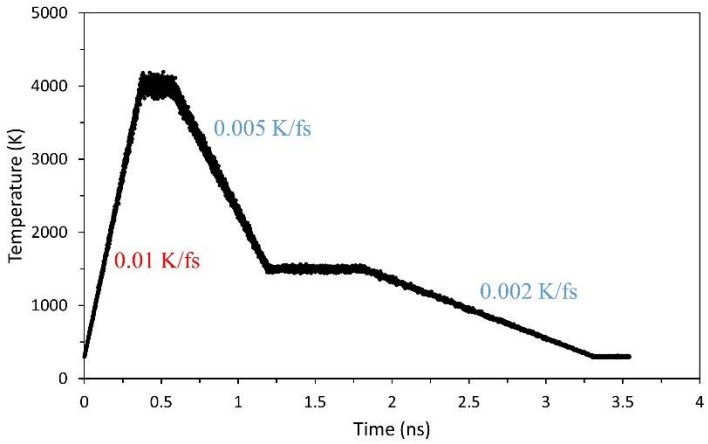

Figure 4.1: Temperature vs simulation time during the amorphous silica creation process. Crystalline cristobalite was heated from 300 K to 4000 K at 10 K/ps heating rate, then the liquid was brought back to room temperature in two stages at 5 K/ps cooling rate.

The model system, shown in Figure 4.4, consisted of 50 cyclohexene molecules confined between two amorphous silica slabs. The number of cyclohexene molecules was chosen to form at least a monolayer coverage on the surfaces. The creation of the amorphous silica slabs involved using the heating and quenching method[38,50,84] that involved heating up crystalline cristobalite from 300 K to 4000 K at 0.01 K/fs and then cooling it down to room

temperature in two stages as shown in Figure 4.1. Bulk cristobalite (periodic boundaries in all three directions) was heated to 4000 K with a heating rate of 0.01 K/fs, followed by a 200 ps equilibration at 4000 K. Then the liquid was cooled down to room temperature in three steps: 4000 K to 1500 K at 0.005 K/fs rate, followed by a 250 ps equilibration at 1500 K, and finally, 1500 K to 300 K at 0.002 K/fs rate. A vacuum region was placed on two sides of the bulk cristobalite during the amorphization process to achieve a silica slab with an average roughness of ~2 Å. The slab was then equilibrated at 300 K and truncated from one side to have thickness of ~20 Å. The final dimensions of the amorphous slabs were about 20 Å thick and 33x32 $Å^2$ in the lateral direction. The physical properties of the amorphous slabs are reported and compared with literature in Table 2, while the density profile of the slab and different radial distribution functions are shown in Figure 4.2, and Figure 4.3, respectively. Finally, the slab was duplicated, and the two resulting silica surfaces oriented as shown in Figure 4.4.

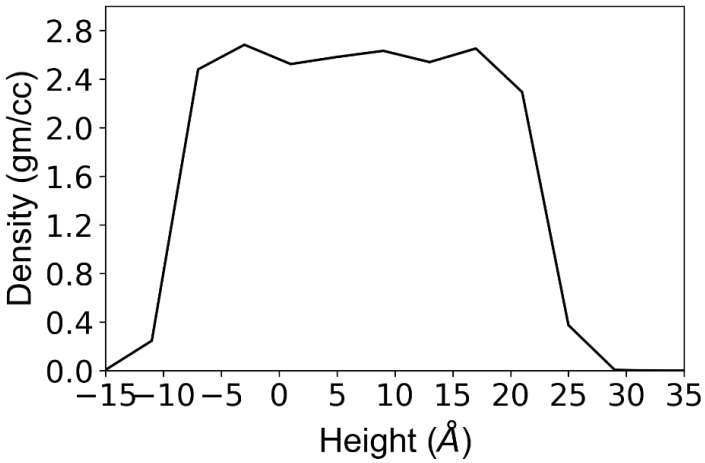

Figure 4.2: Density profile of the amorphous silica slab. From left to right in the x-axis, the density of the amorphous silica slab at the bottom quickly reaches the bulk average density of 2.5 gm/cc and again falls back to zero in the surface region.

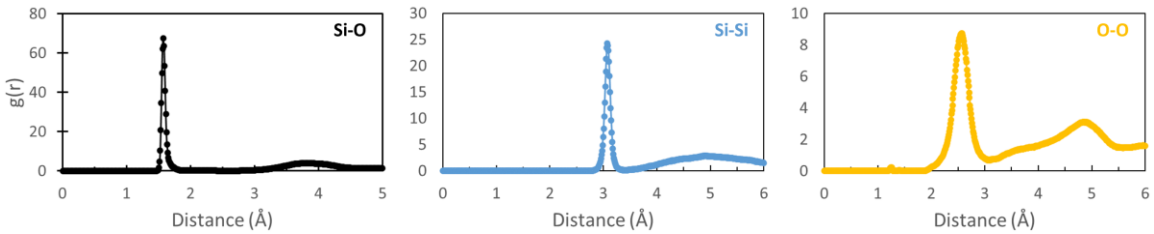

Figure 4.3: Si-O, Si-Si, and O-O radial distribution function (RDF) of the amorphous silica slab. The first peak position of the Si-Si, Si-O, and O-O RDF is, respectively, at 1.58 Å, 3.07 Å, and 2.59 Å.

The two silica slabs were initially placed 20 Å apart. This arrangement aimed to minimize interactions between the slabs, allow enough space for the cyclohexene molecules to equilibrate without mechanical stress, and minimize the computational time required to bring the slabs together. Silica atoms located at the bottommost 5 Å of the lower slab and the uppermost 5 Å of the upper slab were treated as rigid bodies. The initial dimensions of

the simulation box were 33 x 32 x 71 Å^3, with periodic boundary conditions in the x- and y-directions and fixed boundaries in the z-direction. The canonical ensemble (NVT) was applied to all non-rigid atoms, and charge equilibration was performed throughout the simulation.

A three-step procedure was followed for each MD simulation. First, energy minimization of the simulation system was performed using a conjugate gradient algorithm followed by dynamic equilibration at 300 K. Then, the upper slab was moved towards the bottom slab in the z-direction until the average distance between the slabs was approximately 10 Å. Next, the system was compressed at pressures of 1, 2, 3, or 4 GPa by applying load on top of the upper slab for 100 ps to let the system equilibrate at the desired pressure. Finally, sliding simulations were carried out by moving the upper slab at a speed of 10 ms^{-1} in the x-direction for 2 ns while keeping the normal load unchanged. Although the sliding speed used in the simulations is orders of magnitude higher than in the tribometer experiments, such sliding speed is routinely used in reactive MD simulations to minimize the computational cost. Simulations were repeated to get four independent trajectories at each pressure condition.

Table 2: Physical properties of the amorphous silica and comparison with literature

	This study	Khajeh 2018[38]	Experimental[86–88]
Bulk density (gm/cc)	2.5	2.1	2.2
Si-O RDF 1st peak (Å)	1.58	1.58	1.62
Si-O-Si (Degree)	150.2	152.0	144, 153
O-Si-O (Degree)	108.9	110.5	109.5
Si-Si RDF 1st peak (Å)	3.07	-	3.06
Si-Si RDF 2nd peak (Å)	4.95	-	5.2
O-O RDF 1st peak (Å)	2.59	-	2.53
O-O RDF 2nd peak (Å)	4.87	-	4.90

4.2.2 Nudged Elastic Band Methods

The energy barriers for oxidation and oligomerization reactions were computed using NEB calculations.[89–91] The NEB calculations were performed using LAMMPS with the same ReaxFF potential as in the dynamic simulations. The NEB method calculates the Minimum Energy Path (MEP) for any transition by optimizing intermediate images or replicas along the reaction path.

The NEB calculations were performed with a total of 50 replicas, including the initial and final replicas. The replicas were connected by virtual springs to ensure equal spacing between them. Another spring perpendicular to the transition path was applied to maintain a straight path for transition. The total force acting on a replica was the combination of the

spring force along the tangent to the replica on the reaction path, the true force perpendicular to the tangent, and the perpendicular component of the spring force regulated by a switching function.[90,92] The series of replicas was converged to the MEP by minimizing the total force acting on each of the replicas through damped dynamics until a force criterion of 0.1 eV/Å was met for the saddle point.[91–93] The NEB calculations incorporated the climbing image method, where the replica with the highest energy was driven to the top of the energy barrier to maximize its energy.

Two sets of calculations were performed. In the first, the initial and final replicas for the NEB calculations were obtained directly from the reactive MD simulations. All silica atoms and cyclohexene molecules except for those directly relevant to the reaction were deleted from the simulation to create the initial and final replicas for the NEB calculations. The initial and the final replicas were energy minimized and structurally optimized in LAMMPS prior to the first set of NEB calculations. Then, a second set of calculations was performed for deformed cyclohexene. In this set, the structurally optimized cyclohexene molecule in the initial replica was systematically deformed by compressing or extending one or more specific bonds.

4.3 Results and Discussion

In the VPL experiment performed by Yu-Sheng Li and Dr. Seong H. Kim, products with low vapor pressure remain on the surface, while species with high vapor pressure, such as unreacted cyclohexene adsorbates or small fragments, evaporate into ambient air during the tribotest. The yield of products that remain on the surface after the tribotest can be measured from the AFM tapping mode images. Figure 4.5 shows the semi-log plot of normalized yield vs. shear stress from these experiments. The increase of yield with shear stress and the negligible temperature rise[85] confirm this is a stress-activated reaction. Since only the mechanical energy term in Equation (1) depends on shear stress, the slope of the line in Figure 4.5 can be used to calculate the mechanical energy E_m to be between 0.1 kcal/mol and 0.2 kcal/mol for the range of shear stresses in the experiments.

EDX mapping revealed that the tribopolymer contains a significant amount of oxygen, although the precursor (cyclohexene) does not have any oxygen (see inset to Figure 4.5). There are three possible origins. One is the involvement of surface oxygen in tribochemical reactions. The second is the oxidation of intermediates due to a trace amount of O_2 and H_2O in the nitrogen carrier gas. In fact, when the carrier gas was switched to O_2, the reaction yield was observed to increase.[85] The third is post-test oxidation of chemically-unstable tribopolymers by ambient air during the sample transfer from the environment-controlled tribotesting unit to the EDX system. Although the current experiment cannot determine which is the main mechanism, previous reactive MD simulations suggested that the involvement of surface oxygen is likely to occur.[50] In fact, we have observed wear of the substrate when tribochemical polymerization of cyclohexene takes place under the sliding conditions, whereas no wear is observed in the absence of tribochemical polymerization.[85,94]

Atomistic details of the initial stages in the cyclohexene polymerization reactions were investigated with reactive MD simulations. These reactions were found to proceed in two steps:[50,84] oxidative chemisorption (corroborated by the EDX results) followed by oligomerization (specifically the formation of dimers, trimers, etc.) that are assumed to be

the first step of tribopolymerization observed experimentally. Figure 4.6 illustrates the decrease in the intact cyclohexene molecules and the concurrent increase in the number of oxidized molecules and oligomers in simulations at 4 GPa normal stress. The number of oligomers was calculated based on the size of the product, e.g., dimers were counted as one, trimers as two, etc. The results of all simulations performed at 1-4 GPa normal stress conditions are shown in Figure A10.

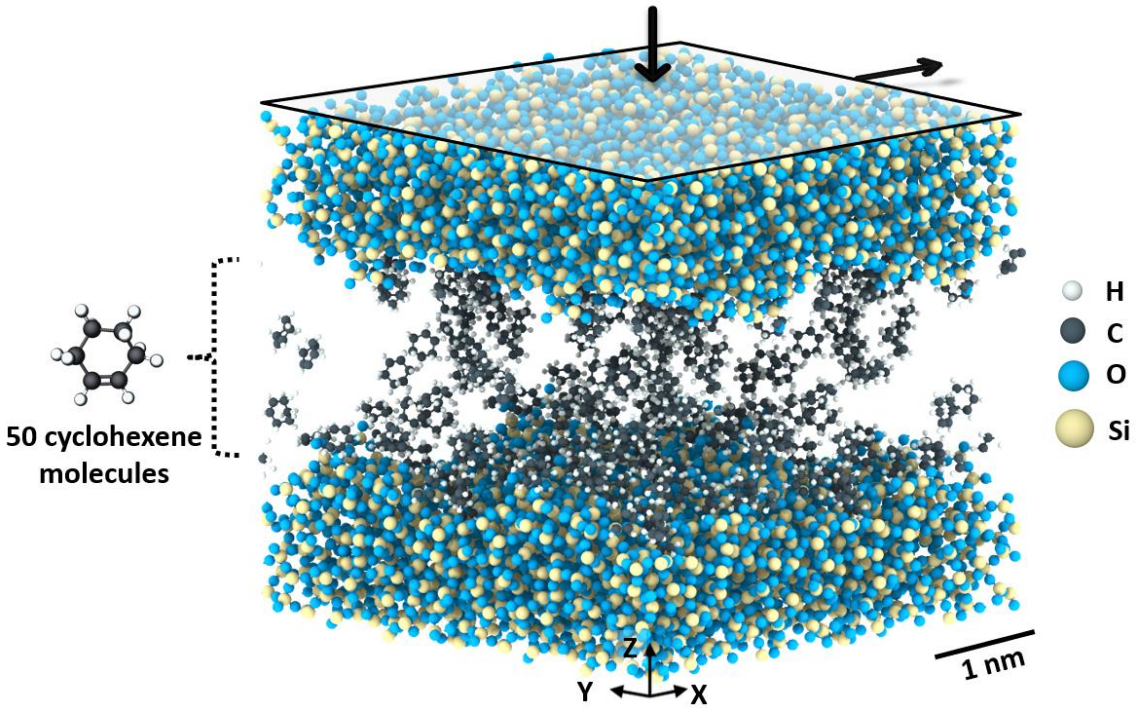

Figure 4.4: Simulation model consisting of two silica slabs and 50 cyclohexene molecules. The white, black, blue, and yellow spheres represent hydrogen, carbon, oxygen, and silicon atoms, respectively. The arrows show the direction of the applied normal and shear stress.

Approximately 10 cyclohexene molecules underwent oxidative chemisorption reactions even before any mechanical stress was applied during the initial thermal equilibration stage in the first 0.1 ns of a simulation (Figure 4.6, Figure A10b) due to the presence of reactive sites on the silica surfaces. After the initial 0.1 ns, normal stress was applied to the system and the cyclohexene molecules were compressed to the desired pressure. The application of normal stress resulted in a small increase in the chemical reactivity in the system. However, normal stress alone induced fewer than five oxidative chemisorption reactions (Figure 4.6, Figure A10b) and fewer than three oligomerization reactions (Figure 4.6, Figure A10c) in most simulation cases. A previous study on α-pinene investigated the effect of normal stress on similar oxidative chemisorption and oligomerization reactions and showed that, as seen here, normal stress alone was not a key driver of these reactions.[50]

In contrast, the application of shear stress at around 0.35 ns led to a notable increase in all reaction kinetics. With shear stress, the reduction of intact cyclohexene (Figure 4.6, Figure A10a) and the production of oligomers (Figure 4.6, Figure A10c) followed an exponential decay curve, indicating first-order kinetics. The temporal change of intact molecules in

simulations was fitted with an exponential function to calculate the reaction rate constants for the consumption of intact reactants (Figure A10). Shear stress was averaged over the last 1.5 ns of each simulation when the friction in the system reached a steady state after an initial run-in stage (Figure A11). Then, as was done with the yield of the polymerization reactions in experiments, we plotted the natural log of the reaction rate constant as a function of shear stress (Figure A12). The reaction rate constant, *k*, was calculated by fitting the temporal change of the number of unreacted precursor molecules in the simulation to the first order kinetics equation, as shown in Figure A10a. Shear stress, τ, in the simulation was calculated from the shear stress on the upper slab, as shown in Figure A11. The reaction rate constants increased exponentially with increasing shear stress, which confirmed that the oxidative chemisorption and oligomerization reactions were stress-assisted. The mechanical energy E_m was calculated from the slope of a linear fit to the reaction rate constant vs. shear stress data (Figure A12) and was found to be between 0.4 kcal/mol and 1.8 kcal/mol with shear stresses ranging from 0.7 GPa to 2.2 GPa.

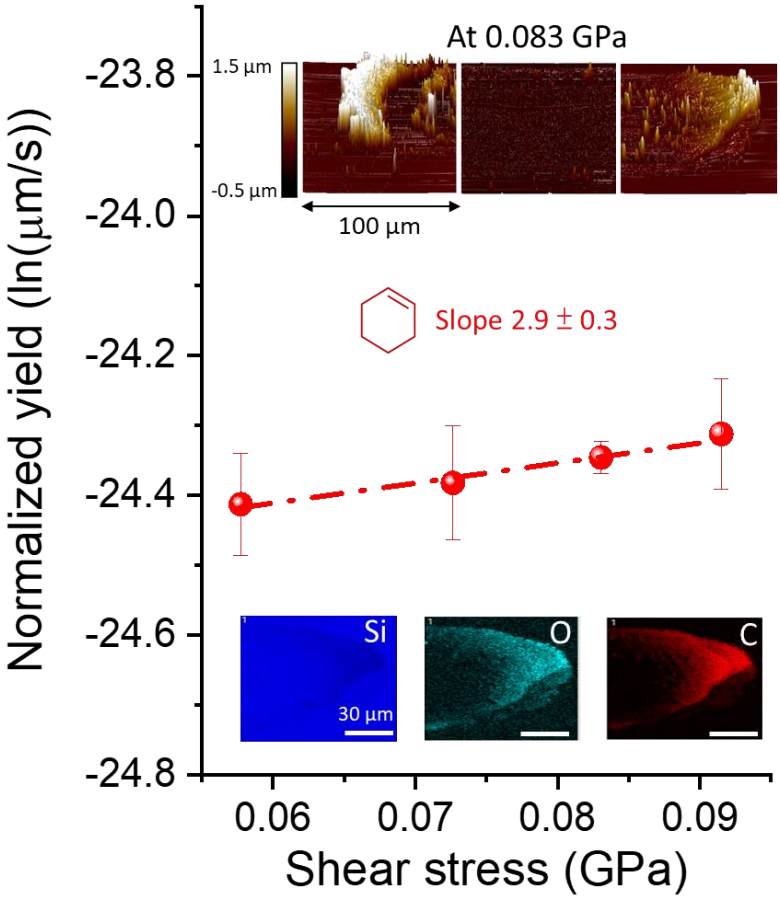

Figure 4.5: Semi-log plot of the normalized yield to shear stress for tribopolymers produced from cyclohexene in N_2. Insets show AFM images of the left, middle, and right sides of the wear tracks, along with EDX mapping of the tribopolymer. Error bars represent the standard error of mean obtained from three different sliding tracks. The figure and all its contents were provided by Yu-Sheng Li and Dr. Seong H. Kim.

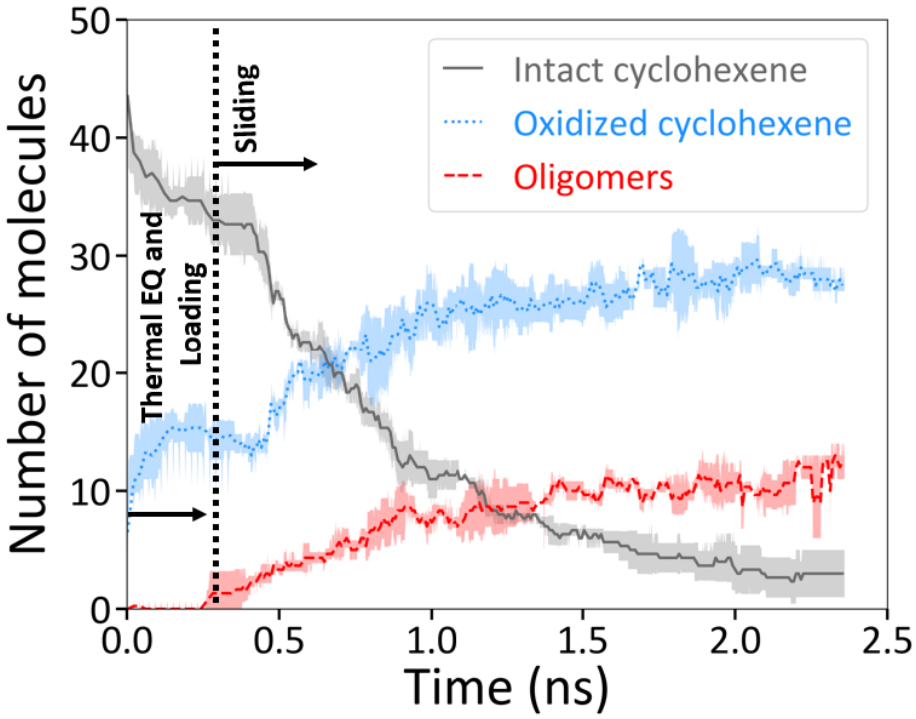

Figure 4.6: Evolution of intact cyclohexene molecules and reaction products in simulations at 300 K and 4 GPa normal stress. The number of intact cyclohexene molecules in the system decreased as the molecules underwent oxidative chemisorption or oligomerization reactions. Simulations were repeated four times at 4 GPa, and the lines represent the average of four simulations. The shaded regions represent one standard deviation from the average. The sliding process started at ~0.35 ns.

The mechanical energy contribution lowering the effective activation energy is larger in the simulation than the value determined in the experiments. However, considering the large difference in sliding speed, system scale, and the number of reactants, the observed discrepancy is relatively minor. In addition to scale, there are several other factors that could contribute to the difference in mechanical energy. First, the experimental value was calculated using the average contact stress estimated from the Hertzian contact mechanics because the distribution of local contact stress due to the surface roughness could not be determined. Second, once tribopolymers were produced in experiments, not all of them could be pushed out to the ends of the sliding track (see Figure 4.5) and some would remain in the track. The latter could affect the adsorption isotherm of cyclohexene to the surface and be involved in subsequent reactions. Lastly, the mechanical energy calculated in the simulations was for the "consumption" of monomers, but that obtained in the experiment was for the "production" of polymeric species. Not all cyclohexene molecules activated by oxidative chemisorption end up forming oligomers; some of them must have desorbed back into the gas phase during the interval between consecutive sliding cycles. Despite the difference in the absolute values of E_m, a similar trend in reaction yield or rate constant with respect to shear stress suggests that atomistic details found by tracking atomic trajectories in MD simulations are relevant to dynamic processes occurring in the experiment.[35,84]

The shear stress dependance of the cyclohexene oligomerization is consistent with the previous studies where such mechanochemical oligomerization or polymerization of organic molecules at sliding interfaces has been shown to be primarily shear driven.[49,85,95] Previous reactive MD simulations have shown that oligomerization of allyl alcohol and α-pinene were driven by shear stress.[35,38,50] The effect of normal and shear stress was further decoupled in case of α-pinene using reactive MD simulations by applying cyclic normal load which showed that normal stress alone could not drive chemical reactions.[50] Shear sensitivity has also been observed for commercially used organic molecules with complex chemical structure. Polymerization of zinc dialkyl dithiophosphate or tricresyl phosphate on various metallic and non-metallic surfaces during rubbing motion has been shown to follow the Bell model where the primary stress component to drive the reactions was shear stress.[30,31,33,52,70] While it is evident that shear stress can effectively activate organic molecules to undergo oligomerization reactions, the mechanism through which shear activation happens requires further investigation.

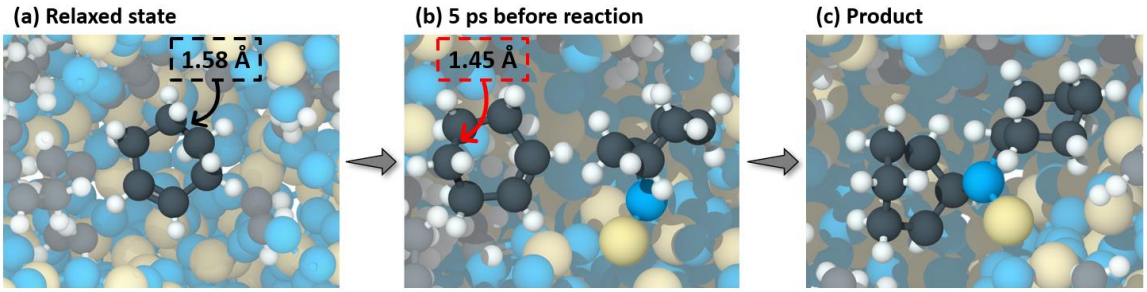

Figure 4.7: Simulation snapshots of an intact cyclohexene molecule showing a series of events that led to an oligomerization reaction. (a) The intact molecule in relaxed state where all bond lengths and angles were close to their equilibrium values. The length of one of the C-C bonds at the relaxed state was ~1.58 Å. (b) The intact molecules within 5 ps prior to oligomerization. The previously mentioned C-C bond was deformed by shear and its length decreased to ~1.45 Å just before the reaction happened. (c) The deformed molecule reacted at the C=C double bond with an oxidized molecule and formed a dimer.

To understand the mechanisms of shear-activation, reactions between intact cyclohexene molecules and chemisorbed cyclohexene molecules were monitored to determine the reaction pathway. Snapshots of a representative reaction are depicted in Figure 4.7 and the corresponding chemical equation for the reaction is provided in Figure A13. Previous reactive MD simulations have shown that shear-driven oligomerization reactions of cyclohexene on silica involve direct activation of the C=C bond.[84] Similar reaction pathways were observed in this study where the carbon atoms of the double bond reacted with a chemisorbed molecule (Figure 4.7b) to create an ether linkage and consequently produce an oligomer (Figure 4.7c). The molecular structure of the intact cyclohexene molecule participating in oligomerization reactions was closely analyzed throughout the reaction process to detect deformation. Notably, within 5 ps of product formation, one of the C-C bonds opposite to the C=C bond in the cyclohexene became visibly distorted compared to the thermally relaxed molecule (Figure 4.7b).

To substantiate the findings, the distribution of bond lengths in the cyclohexene molecules within 5 ps of an oligomerization reaction were compared with the bond length

distributions for the cyclohexene molecules at thermal equilibrium (Figure 4.8). This analysis has been previously used to detect molecular deformation of allyl alcohol and α-pinene.[35,38] Here, the carbon atoms in cyclohexene were numbered from 1 to 6 according to the IUPAC convention, where C1 and C2 correspond to the carbon atoms at the double bond site. Since the cyclohexene molecule is symmetrical, data for C2-C3 and C6-C1 bonds, and C3-C4 and C5-C6 bonds were combined to create one distribution for each pair of bonds (see insets to Figure 4.8).

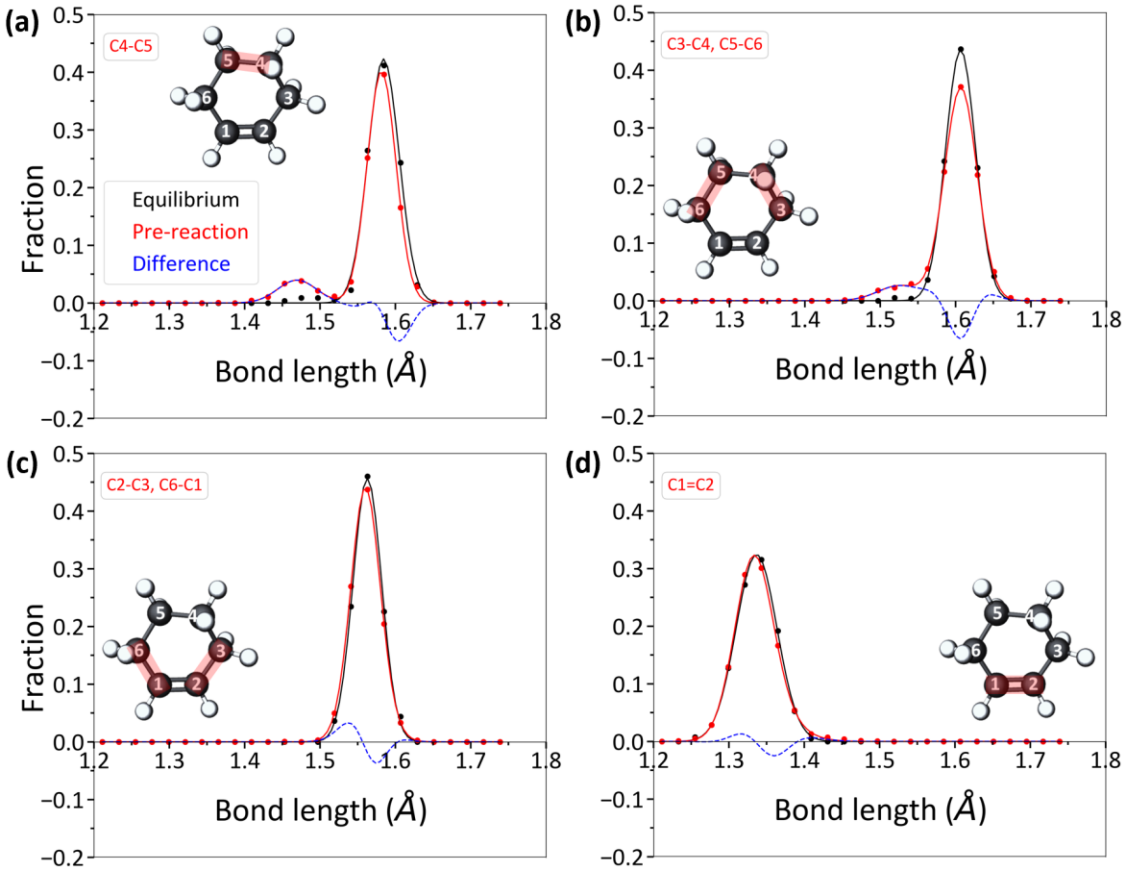

Figure 4.8: Bond length distributions of cyclohexene molecules at equilibrium (black distributions) and prior to oligomerization reactions (red distributions). The equilibrium distributions were calculated from intact cyclohexene molecules in the first 50 ps of simulation during which no mechanical stress was applied. The red distributions were calculated from intact cyclohexene molecules that were within 5 ps of participating in an oligomerization reaction. The blue dotted lines show the difference between the red (pre-reaction) and black (equilibrium) distributions.

In Figure 4.8, the blue dashed lines highlight the difference between the equilibrium and pre-reaction bond length distributions, where a positive value means there were more bonds with a given length just before the reaction than at equilibrium. The blue dashed line for the C4-C5 bond shows an increased population at 1.46 Å, which is shorter than the average equilibrium bond length of 1.58 Å. This indicates this bond was compressed just before reaction (Figure 4.8a). Note that the ReaxFF forcefield utilized in this study slightly overestimated the average equilibrium bond length of the C-C single bonds in

cyclohexene.[96] The distribution for C3-C4 and C5-C6 bond lengths exhibited a shoulder peak around 1.52 Å (Figure 4.8b), indicating these bonds too were compressed slightly before the reaction. The C2-C3 and C6-C1 bonds, adjacent to the double bond, did not exhibit an appreciable change in length (Figure 4.8c). Similar trends in bond length distributions were observed in the bond-by-bond analysis for oxidative chemisorption (Figure A14). Note that this analysis was only carried out for the intact cyclohexene molecules since the chemisorbed molecules already exhibited non-equilibrium structures so there was no reference state.

Although the C1=C2 double bond site was the most reactive under shear, the C1=C2 bond length distribution prior to reactions was similar to the equilibrium distribution (Figure 4.8d) and did not show any signs of deformation. However, physical deformation leading to mechanochemical activation may or may not involve the stress-activated bond. For example, the physical deformation required for the mechanochemical decomposition of methyl thiolate occurred at the angle between the surface and the scissile S-C bond.[18] Mechanochemical activation of spiropyran was shown to involve the deformation of dihedrals in the vicinity of but not directly at the scissile C-O bond.[97] A similar effect has been observed for polymers where the accumulation of strain in dihedrals facilitated bond dissociation.[98] Further, the shear-activation of the C=C double bond of α-pinene has been shown to be triggered by deformation of C-C bonds or dihedrals at the four membered or six membered ring.[38,50] So, the role of deformation in mechanochemical activation may not be to directly weaken the reacting bond, but rather to alter the potential energy surface of the reactant molecule such that a specific bond or chemical feature can be easily activated.

To quantify how much the reaction energy barrier was reduced by molecular deformation, NEB calculations were conducted for oligomerization reactions using undeformed and deformed cyclohexene molecules. The NEB calculations were performed with the ReaxFF potential such that the results could be directly correlated to observations from the ReaxFF MD simulations. The initial reactant state and the final product state of the NEB calculations are shown in Figure 4.9a and representative NEB-calculated MEPs for undeformed and deformed cyclohexene molecules are shown in Figure 4.9b. Since deformation was mostly observed in the C3-C4-C5-C6 side of a reactant cyclohexene molecule in Figure 4.8 and Figure A14, the NEB calculations were performed with the C3-C4, C4-C5, or C5-C6 bond deformed by ±0.01 Å up to a maximum of ±0.06 Å.

The mechanical energy (E_m) determined from the slope in the semi-log plot of reaction rate constant vs. the shear stress is the difference between the change in reactant energy ΔE_r and the change in transition state energy ΔE_{ts} due to mechanical stress, which can be expressed as:

$$E_m = \Delta E_r - \Delta E_{ts} \tag{4}$$

An increase in reactant energy or a decrease in transition state energy could cause an increase in the total mechanical energy. For the representative NEB calculation with deformation shown in Figure 4.9b, where the C5-C6 bond was compressed by 0.06 Å, the reactant energy increased by ΔE_r = 3.1 kcal/mol and the transition state energy increased by ΔE_{ts} = 1.2 kcal/mol, such that the total mechanical energy was 1.9 kcal/mol. This is the amount by which the thermal activation energy was decreased by shear-induced

deformation of the molecule. To determine if this trend was generalizable, we calculated E_m and ΔE_r for all unique bonds in the cyclohexene molecule deformed from compression to tension (Figure 4.9c). The plot exhibits a linear relationship with a slope of ~0.81 (R^2 = 0.93) between E_m and ΔE_r. The strongly positive correlation confirms that most of the mechanical energy is attributed to an increase in a reactant state energy. The slope being slightly below unity shows that deformation also increases the transition state energy, albeit much less than the amount by which the reactant energy increases. An increase in the reactant energy and a smaller increase in the transition state energy due to reactant deformation has also been captured in DFT calculations of [4+2] Diels-Alder cycloadditions between anthracene and dienophiles under normal stress.[20]

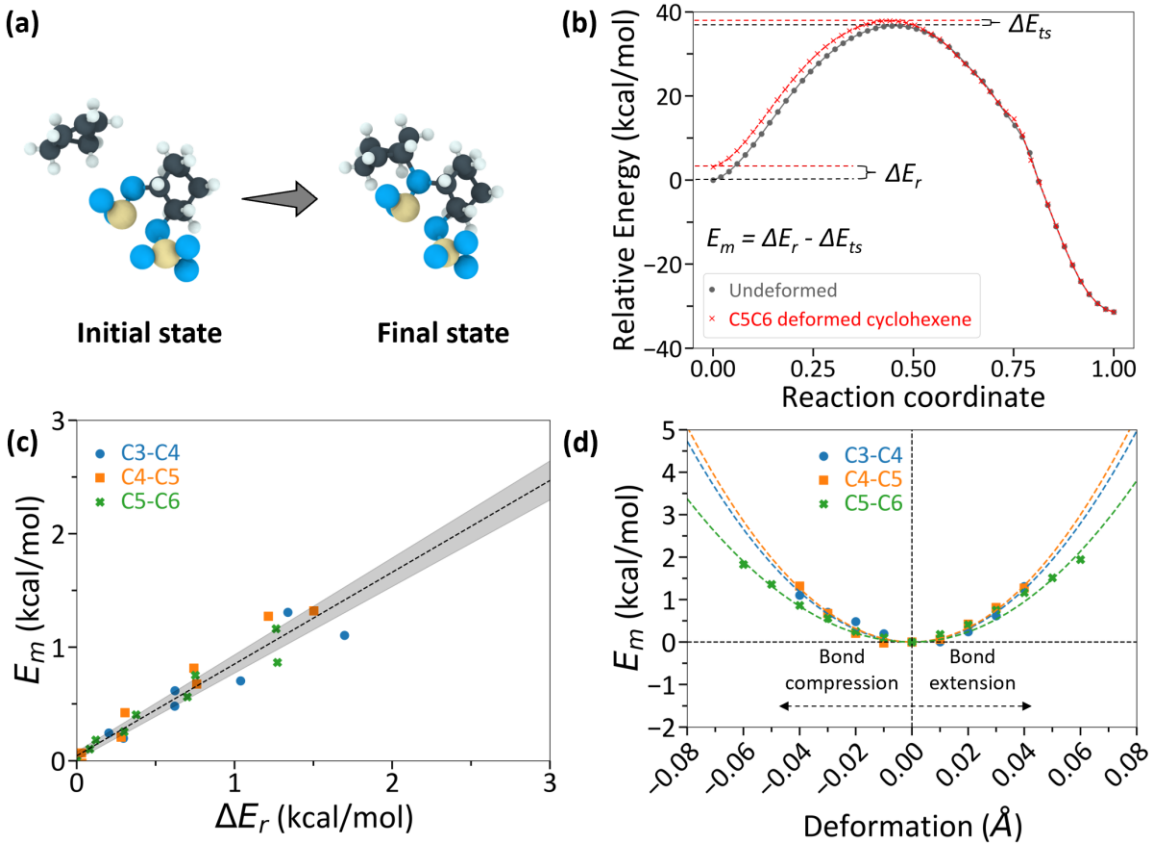

Figure 4.9: NEB calculation results for a representative oligomerization reaction. (a) The initial and final states of an oligomerization reaction used for NEB calculations, (b) Representative NEB-calculated MEP for structurally optimized, undeformed cyclohexene molecule (black) and for deformed cyclohexene molecule (red). For the deformed case, the C5-C6 bond of the intact cyclohexene molecule was compressed by ~0.06 Å from the average equilibrium bond length. Variables are defined in the text. (c) Mechanical energy, E_m, vs. change in reactant state energy, ΔE_r, from NEB calculations. Each data point represents an individual NEB calculation with compressive deformation to a specific bond. The fitted dashed line had an R^2 value of 0.93 and a slope of ~0.81, suggesting that $E_m \approx \Delta E_r$. (d) NEB calculated reduction in energy barrier, E_m, for a range of deformed bond cases. E_m increased quadratically (dashed lines show quadratic fit) with increasing bond deformation.

Figure 4.9d illustrates the relationship between the mechanical energy from an NEB-calculated MEP and the amount of deformation introduced to individual C-C bonds in the reactant molecule. The mechanical energy varied quadratically with the amount of deformation in each C-C bond. As the deformation applied to the C-C bonds in the NEB calculations was small (<0.1 Å) and no bonds dissociated in the deformed reactant molecule, the reactant molecule was modeled as a Hookean spring. Then, the mechanical energy could be considered as the energy stored in a spring subject to axial deformation. Such modeling approach using Hooke's law has previously been used to explain the deformation behavior of mechanophores under applied stress.[99,100] Single molecule force spectroscopy of polymer chains using AFM has shown that at small deformation (~ less than 0.3 strain) the stretching of a polymer chain could be modeled using Hooke's law.[99,100] Consequently, the data in Figure 4.9d were fitted with the quadratic potential energy equation of a spring as $E_m = K\Delta x^2$, where Δx is the amount by which a bond is deformed from equilibrium and K is the force constant.

The average force constant obtained from the fitted lines in Figure 4.9d was 9.8 mdyn/Å. Comparatively, the typical force constant for a C-C single bond is about 4 mdyn/Å while, for C=C, it is about 8.8 mdyn/Å.[101,102] Our calculated force constant was higher than the force constant reported for single bonds. However, the deformation of a C-C bond in the reactant cyclohexene molecule resulted in deformation of the adjacent bonds as well as bond angles in the NEB calculation, so the stored energy was associated with deformation of the entire molecule with a force constant larger than that of individual bonds. Regardless, the close agreement between the calculated and expected force constants suggests that the contribution of shear stress to mechanical energy can be quantitatively correlated to physical deformation of reactant molecules.

4.4 Conclusions

In conclusion, studying the shear stress-driven reactions of cyclohexene on silica using reactive MD simulations and ball-on-flat tribometer experiments showed that cyclohexene molecules underwent oligomerization or polymerization reactions that followed the typical stress assisted thermal activation model. Reactive MD simulations highlighted the role of oxidative chemisorption in the reaction pathway, an observation that was corroborated by the presence of oxygen in the EDX mapping of the polymer products in experiments.

Results from the reactive MD simulations pointed to stress-induced molecular deformation as the mechanism of mechanochemical activation. Qualitative evidence of deformation was found by visually analyzing intact cyclohexene molecules prior to oligomerization. Deformation was then quantified by comparing all C-C bonds of the reactant cyclohexene molecules to the corresponding C-C bonds of a cyclohexene molecule in thermal equilibrium. Both visual and quantitative analysis captured physical deformation on the opposite side of the C=C double bond of the six-carbon ring of a reactant cyclohexene molecule prior to shear-driven oligomerization reactions.

The relationship between physical deformation of reactant molecule and mechanical energy in the Bell model was then investigated by a series of NEB calculations of an oligomerization reaction. Comparing the NEB-calculated MEP for all structurally optimized reactants with MEPs for systematically deformed reactant cyclohexene molecule showed that the reactant state energy increased considerably with deformation

while transition state energy remained unchanged or increased only slightly relative to the reactant energy change. Then the NEB-calculated mechanical energy was quantitatively correlated to molecular deformation by modeling the mechanical energy as energy stored in a harmonic spring representing a cyclohexene molecule.

More generally, this study demonstrates the utility of experimentally corroborated reactive MD simulations to capture the dynamic aspects of shear-driven chemical reactions. Since these simulations are computationally efficient enough to model many reactant species sheared by non-ideal surfaces, they provide a means of statistically analyzing reaction pathways and molecular deformation, and a similar approach to that demonstrated here can be used to explore the fundamental mechanisms of other mechanochemical systems.

5 Summary and Future Work

5.1 Summary

This dissertation aimed to study the molecular mechanisms by which shear stress activates reactant molecules. Specifically, shear-driven reactions of α-pinene, methylcyclopentane, cyclohexane, and cyclohexene molecules on silica surfaces were studied to gain atomic scale insights into the mechanisms behind shear-activation.

In Chapter 2, the dissertation investigated the impact of heat and stress on mechanochemical reactions using α-pinene as a model system. At room temperature, α-pinene's reactivity towards oligomerization was minimal without stress but increased with temperature and under shear stress, revealing distinct activation pathways. The findings suggest a novel interpretation of activation volume in mechanochemistry, linking it to molecular deformation induced by shear stress. The study also sheds light on the implications for reaction selectivity and demonstrates the potential of reactive MD simulations in understanding stress-driven chemical reactions.

Chapter 3 focused on studying the mechanochemical activation of methylcyclopentane, cyclohexane, and cyclohexene at a silica interface using reactive MD simulations. The precursor molecules exhibited varying degrees of responsiveness to mechanical activation, with cyclohexene showing the highest reactivity due to its chemical structure. The study underscores how chemical features influence mechanochemical activation modes and provides insights into tuning reactivity by modifying chemical species.

In Chapter 4, the study investigated shear stress-driven reactions of cyclohexene on silica using reactive MD simulations and experimental tribometer studies. The results highlighted the role of oxidative chemisorption in reaction pathways and demonstrated stress-induced molecular deformation as a mechanism of mechanochemical activation. The dissertation concludes by emphasizing the utility of experimentally validated reactive MD simulations in capturing dynamic aspects of shear-driven chemical reactions and suggests avenues for exploring fundamental mechanisms in other mechanochemical systems.

5.2 Future Work

This dissertation made critical contributions to the current understanding of the fundamental mechanisms behind not just shear-driven reactions but also mechanochemical reactions in general. The reactive MD simulations here were designed based on ball-on-flat tribometer experiments and the simulations findings corroborated experimental trends. However, more work has to be done to develop a complete understanding of mechanochemical activation.

Firstly, the reactive MD simulations here explored only four precursor molecules on amorphous silica. The choice of precursor molecules and the surface was mostly limited by the availability of proper reactive forcefield. The chemical features studied in this dissertation included ring strain, C=C double bond, and methyl group. However, it is important to study a larger variety of chemical features which can largely determine the shear sensitivity of a molecule. For instance, secondary sulfur-free zinc dialkylphosphates

(ZDPs) have been shown to grow protective films at faster rates than primary ZDPs.[103] Similar experiments on ZDDP revealed that film growth rates were dependent on the additive's alkyl substituents, where additives with secondary alkyl substituents formed films faster than additives with primary substituents.[33,103] Thus, a homologous series involving primary, secondary, and tertiary alkyl groups can be added to expand this work. Additionally, metallic surfaces such as iron, iron oxides, stainless steel, and copper-based surfaces should also be explored since metallic surfaces are more relevant to real life applications.

Secondly, the reactive MD simulations here were designed to mimic ball-on-flat tribometer experiments. However, the simulations only mimicked inert conditions and did not include any environmental elements like water or oxygen. Ball-on-flat experiments have shown that the frictional behavior, wear, and mechanochemical reactivity of the same precursor molecule on a surface can vary significantly in different environments.[39,58,85] Such differences in mechanochemical reactivity in experiments suggest that the reaction pathways get affected by changes in the environment. Studying the effect of environment on shear-driven reactions is crucial since shear-driven processes in transportation and manufacturing occur in varying environments. So, reactive simulation systems can be designed with oxygen or water molecules at various concentrations along with the precursor molecules to study the effect of environmental species on shear-driven reactions.

Thirdly, the simulations here captured evidence of shear-induced deformation in the precursor molecules before reactions. However, the reactions involved both the precursor molecules and the surface. DFT-based calculations have shown deformation in the surface area where mechanochemical reactions took place.[47] Deformation in the surface could not be analyzed here due to the non-equilibrium state of the amorphous surface during the sliding simulations. Analysis of the deformation in the surface will be the most straightforward with crystalline surfaces. Thus, future reactive MD simulations on shear-driven reactions can be designed with both amorphous and crystalline surfaces to analyze surface deformation. Additionally, the relation between molecular deformation and reduction in the energy barrier found in this study was only limited to small deformation. So, studying larger and more complex molecules, such as TCP or ZDDP, using reactive MD is crucial to find the extent of the relationship.

Finally, the simulated results in this dissertation provided indirect suggestions to the physical meaning of the activation volume term in the Bell model. The physical meaning of activation volume is a highly debated concept in the field of mechanochemistry. Among many ideas, physical deformation of reactant species has been suggested as a possible hypothesis to explain the physical meaning of activation volume. The results from this dissertation also support that hypothesis by demonstrating a direct relationship between molecular deformation and mechanical energy which is proportional to the activation volume. However, the evidence is not fully conclusive since we still cannot explain why large differences in activation volume have been reported for the same chemical system. As such, further investigation is required.

5.3 Concluding Remarks

The importance of shear-driven reactions has been highlighted by the recent experimental findings on tribofilm formation mechanisms, wear mechanisms, and mechanochemical

manufacturing through milling. However, extracting *in-situ* atomic-scale details of the shear-driven processes is inherently challenging using experimental techniques. This dissertation used reactive MD simulations to investigate the molecular mechanisms of shear-driven reactions and made the following contributions to the field of mechanochemistry:

i. Deconvoluted the effect of normal stress and shear stress on shear-driven reactions,
ii. Captured the differences between thermal reaction pathways and shear-driven pathways,
iii. Provided key insights on the effect of chemical features on shear-activation,
iv. Developed a computational method of quantifying molecular deformation,
v. Highlighted the role of molecular deformation in shear-activation,
vi. Established a method of calculating reaction energy barrier under mechanochemical conditions from reactive MD,
vii. And finally, demonstrated a quantifiable relationship between molecular deformation and reduction in energy barrier by shear stress.

The findings from this dissertation will help guide the design of more efficient shear-driven processes and tailor specific molecules for optimum shear-activation. More generally, this work demonstrates the applicability of reactive MD simulations as an investigative tool to study complex mechanochemical systems. The simulation protocols, analysis techniques, and computational methods developed in this dissertation will serve as a strong reference point and guideline for future computational work on mechanical and chemical systems.

Appendix

Supporting Information for Chapter 2: Reactive Molecular Dynamics Simulations of Thermal and Shear-driven Oligomerization

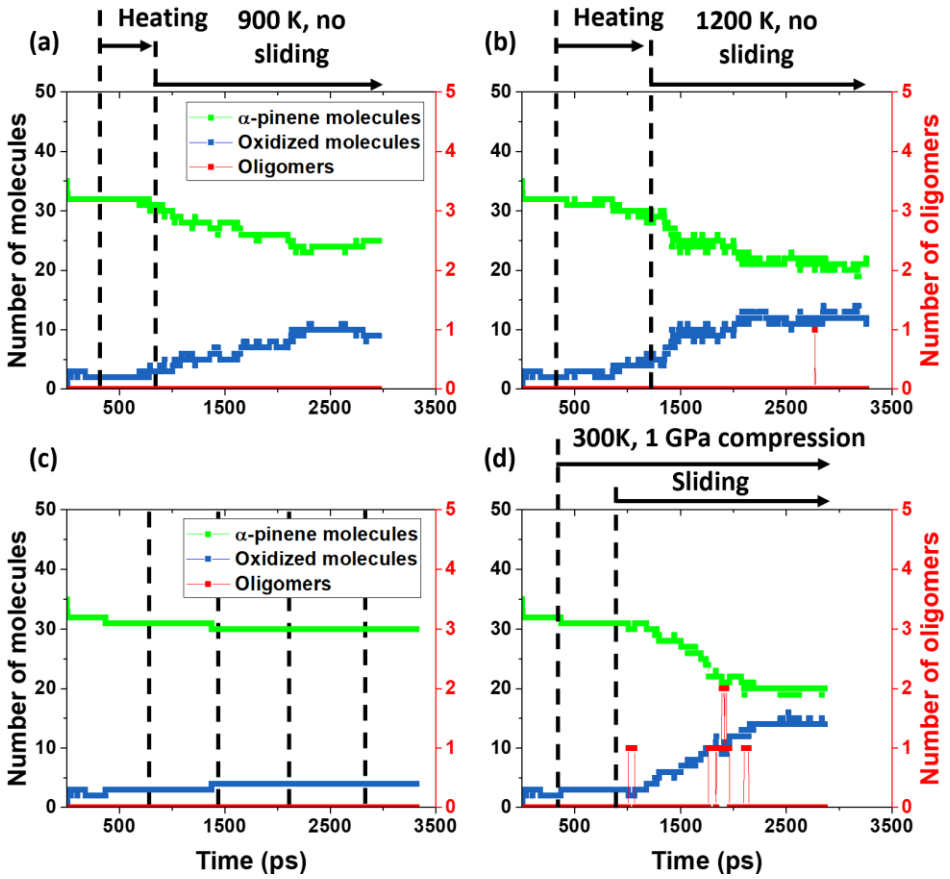

Figure A1: The evolution of different chemical species during the simulations. (a, b) Heating simulations at 900 K and at 1200 K, respectively, without load or sliding. The heating rate from 300 K to the desired temperature was 1 K/ps. (c) Loading at 1 GPa pressure and unloading simulation without sliding at 300 K. The dashed lines represent the beginning of loading cycles for 500 ps followed by unloading by lifting the top slab upwards for 180 ps. (d) 10 ms^{-1} sliding simulation at 1 GPa pressure and 300 K.

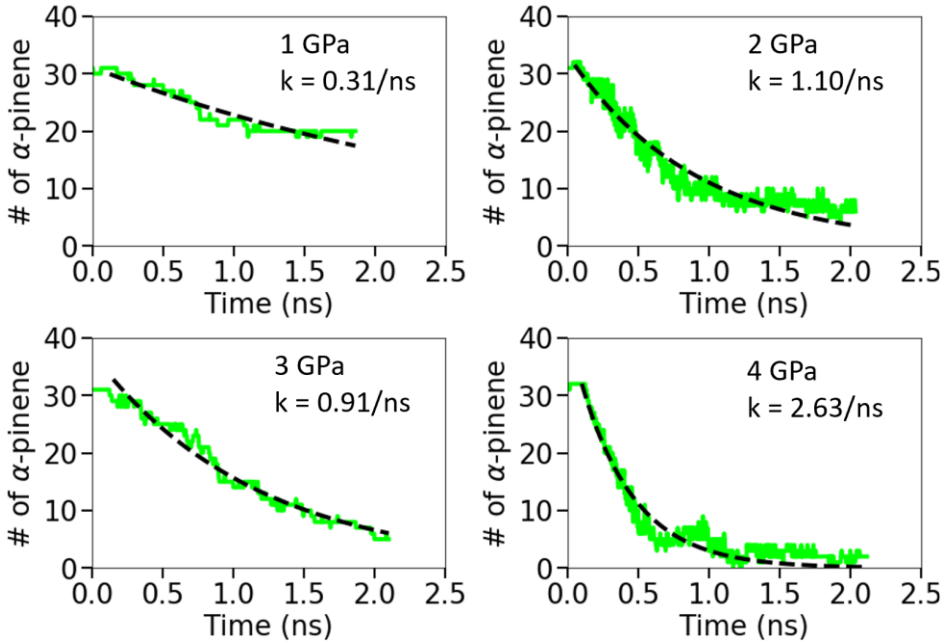

Figure A2: Reaction rate constant (k) for oxidative chemisorption of α-pinene calculated from the first order kinetics in the four sliding simulations at different normal stress conditions. The green lines show the number of intact α-pinene molecules in the sliding simulations and the black lines represent the fits to the first order kinetics. As reactions were driven mainly by shear stress, only the data from the 2 ns of sliding were used for fitting.

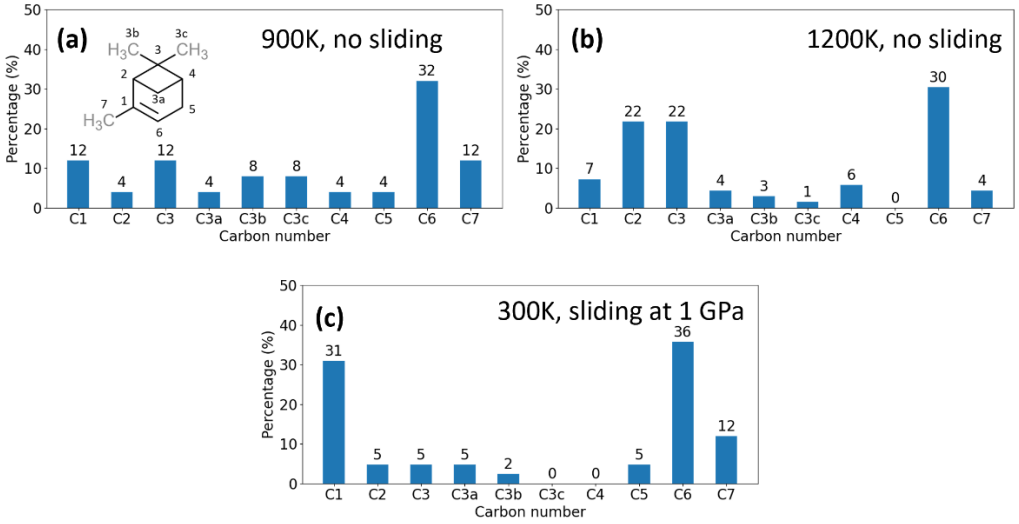

Figure A3: Percentage of oxidation at different carbon sites compared to all unique C-O bonds formed in simulations at (a) 900 K and (b) 1200 K without pressure or sliding, and (b) room temperature with sliding at 1 GPa. At high temperature, carbon atoms in the four-membered ring were more reactive whereas, in the sliding simulation, carbon atoms at the double bond sites were more reactive.

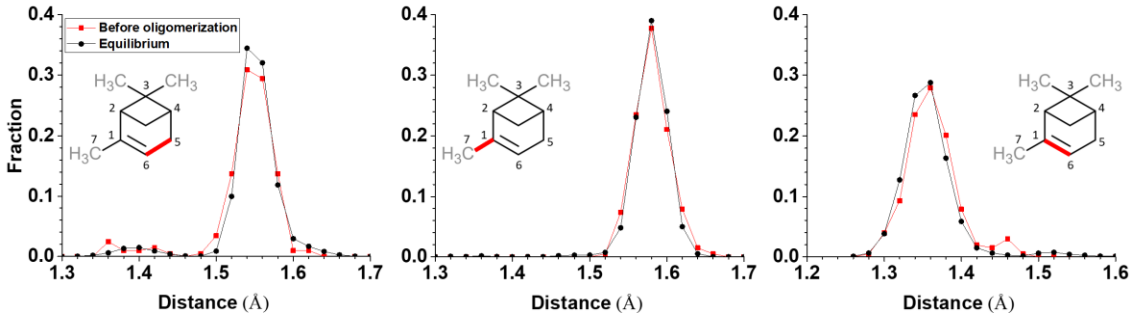

Figure A4: C5C6, C1C7, and C1C6 bond length distributions at equilibrium (black) and before oligomerization through reaction pathway A (red). The red distributions were calculated over 200 ps before a dimeric species formed and averaged over four α-pinene molecules that were the non-oxidized reactants initially (i.e., reacting with the oxidatively chemisorbed species) in pathway A.

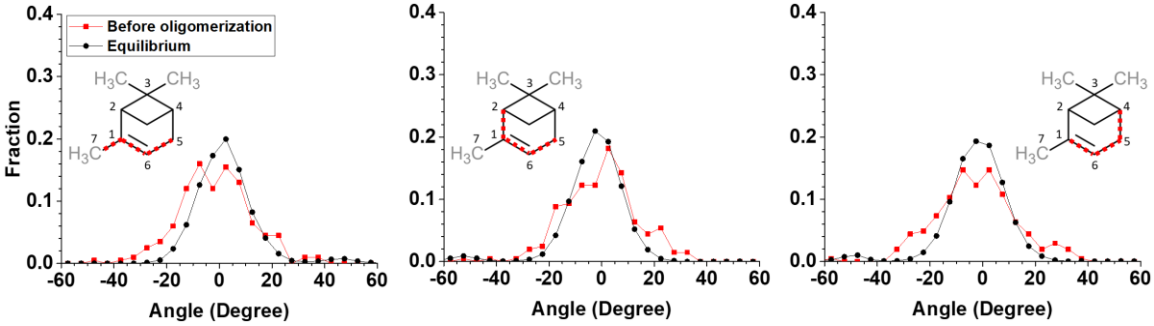

Figure A5: Comparison between bond dihedral angle distributions at equilibrium (black) and before oligomerization through reaction pathway A (red). The red distributions were calculated over 200 ps before a dimeric species formed and averaged over four α-pinene molecules that were the non-oxidized reactant initially (i.e., reacting with the oxidatively chemisorbed species) in pathway A.

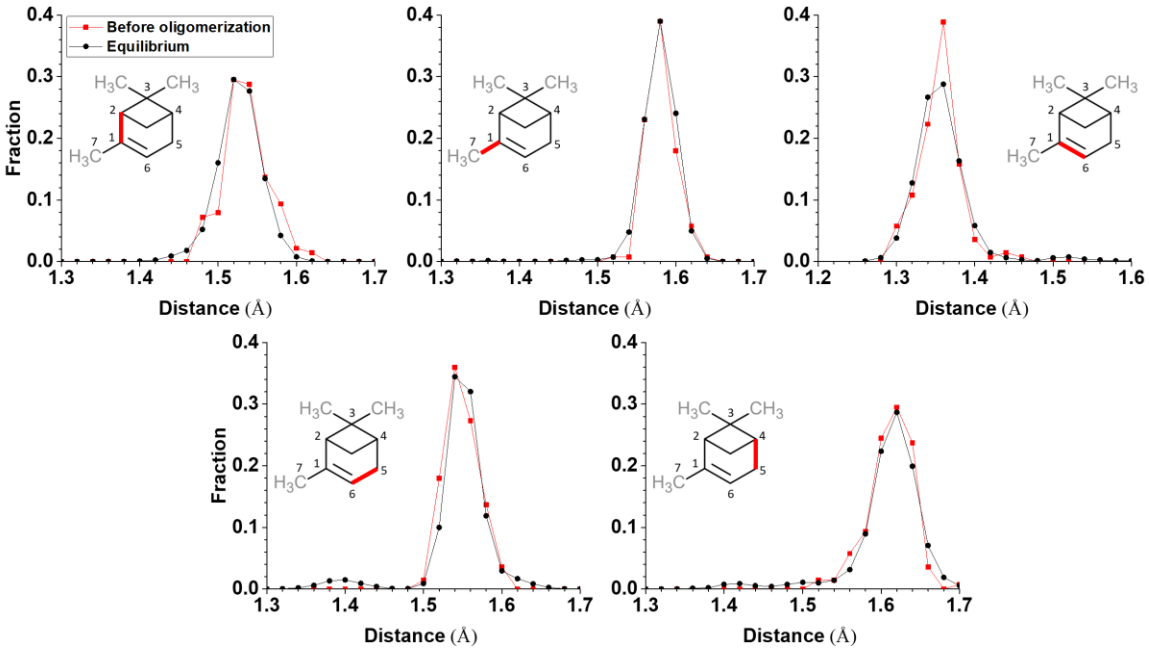

Figure A6: Different bond length distributions at equilibrium (black) and before oligomerization through reaction pathway B (red). The red distributions were calculated over 200 ps before a dimeric species formed and averaged over four α-pinene molecules that were the non-oxidized reactants initially (i.e., reacting with the oxidatively chemisorbed species) in pathway B.

Supporting Information for Chapter 3: Shear-Activated Chemisorption and Association of Cyclic Organic Molecules

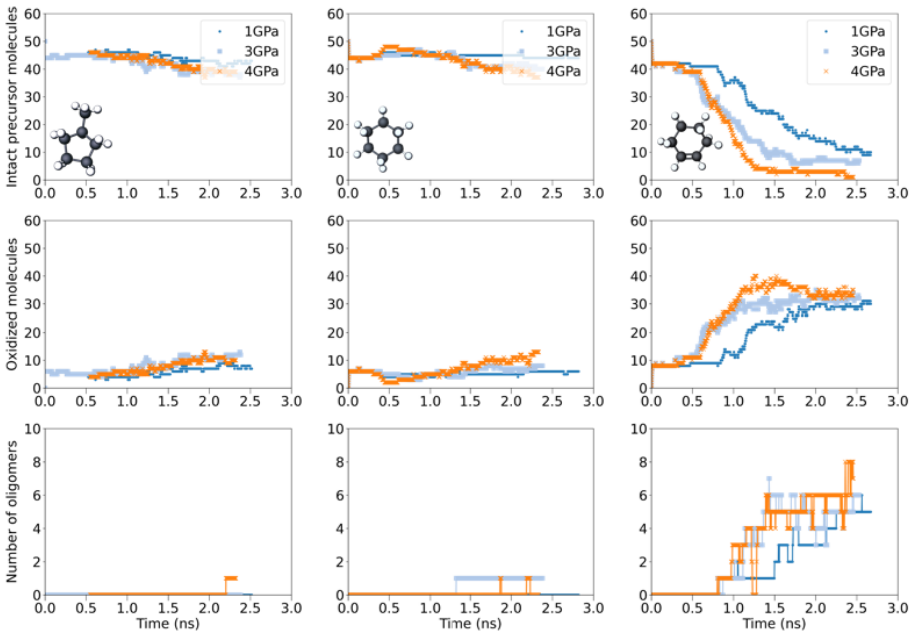

Figure A7: Evolution of the number of intact precursor molecules (top row), corresponding change in the number of oxidized species (middle row), and formation of oligomers (bottom row) in simulations at 1, 3, and 4 GPa and 300 K. Methylcyclopentane (left column) and cyclohexane (middle column) molecules were mostly unreactive while cyclohexene (right column) molecules participated in many shear-driven reactions at any pressure. Sliding started from approximately 0.75 ns, after the system was equilibrated and compressed to the target pressure.

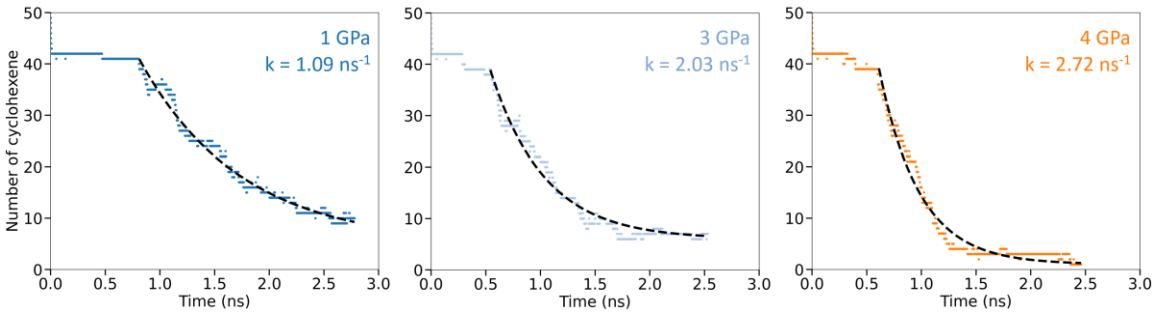

Figure A8: Reaction rate constant (k) for oxidative chemisorption of cyclohexene calculated from the first order kinetics in sliding simulations at 1, 3, and 4 GPa and 300 K. The colored lines show the number of intact cyclohexene molecules in the sliding simulations and the black lines are fits of the data to the first order kinetics equation. As reactions were driven mainly by shear stress, only the data from the 2 ns of sliding were used for fitting.

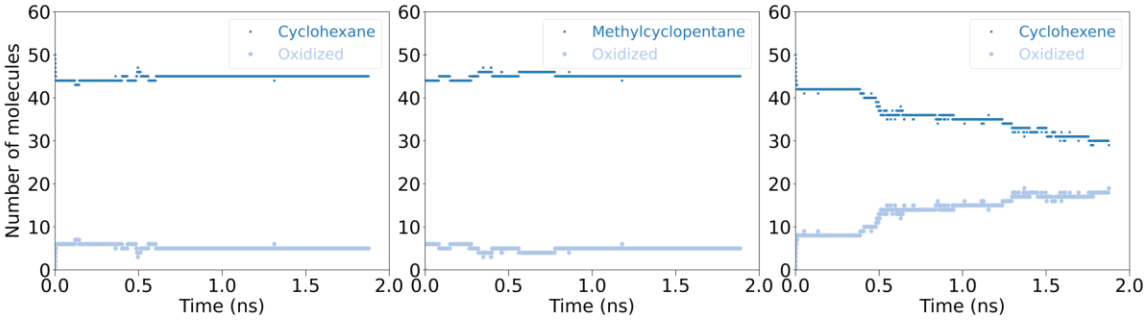

Figure A9: Evolution of the number of intact methylcyclopentane, cyclohexane, and cyclohexene molecules and corresponding change in the number of oxidized species in the heating simulations. The systems were heated from 300 K to 900 K at 1 K/ps heating rate starting from 0.28 ns. The constant temperature simulations at 900 K were run from 0.88 ns.

Supporting Information for Chapter 4: Shear-Activation of Mechanochemical Reactions Through Molecular Deformation

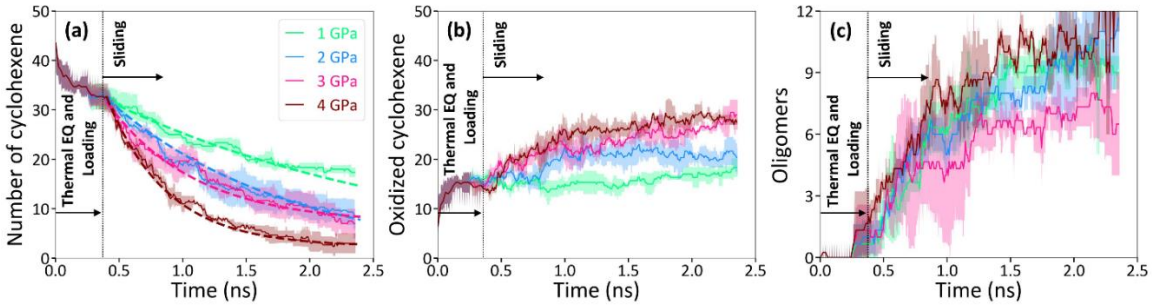

Figure A10: Reaction kinetics analysis from simulations at 300 K and four different normal stress conditions. (a) Decrease in number of intact cyclohexene molecules with simulation time. Evolution of (b) oxidized cyclohexene molecules and (c) oligomers in the simulations. Simulations were repeated four times for each normal stress condition and the solid lines in (a), (b) and (c) represent the average of four simulations. The shaded regions in (a), (b), and (c) represent one standard deviation from the average. The thicker dashed lines in (a) represent fits to the first order kinetics equation.

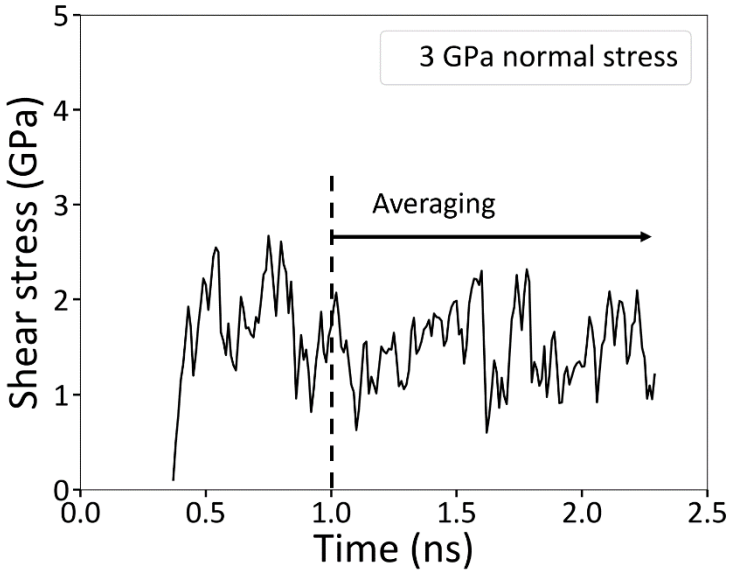

Figure A11: Representative plot of the shear stress in a sliding simulation at the 3 GPa normal stress condition. The average shear stress was calculated from the data after 1.0 ns of sliding.

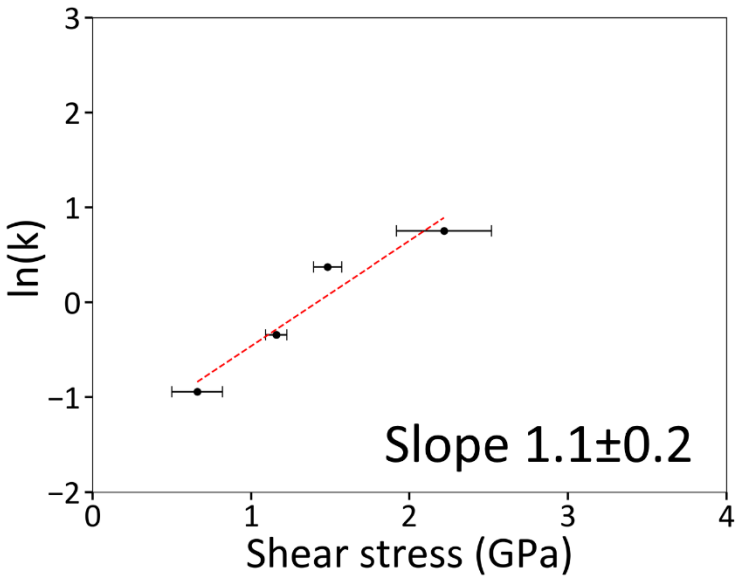

Figure A12: Activation volume for cyclohexene consumption calculated from simulations. The rate constants were calculated from Figure A10, and the shear stresses were calculated from sliding simulations at 1-4 GPa normal stress conditions, as shown by the representative plot in Figure A11. The red dashed line in shows the fit to the Bell model (Equation (3)).

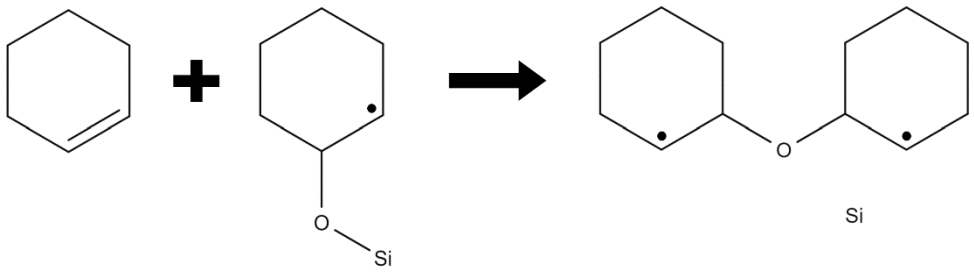

Figure A13: Reaction formula of the chemical reaction shown as simulation snapshots in Figure 4.7; an intact cyclohexene molecule reacting with an oxidized, surface-chemisorbed molecule to form an oligomer.

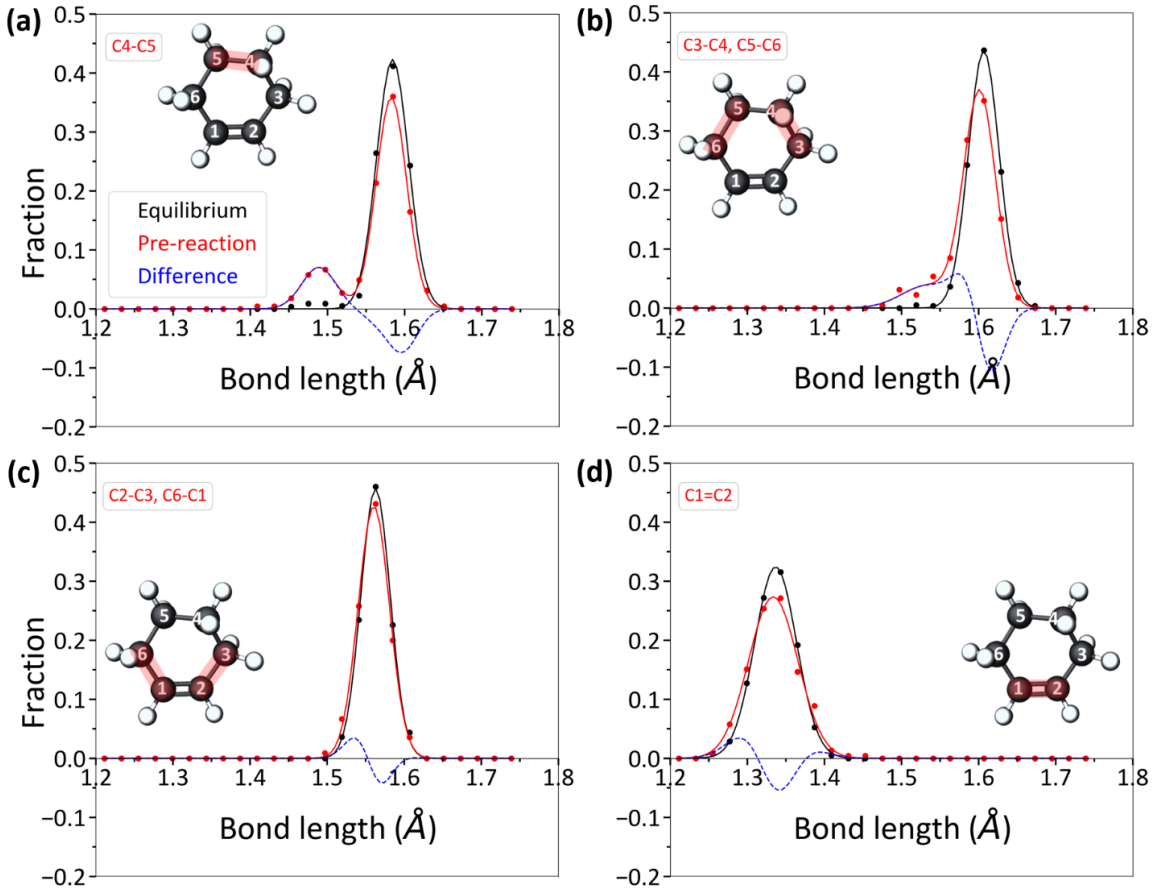

Figure A14: Bond length distributions of cyclohexene molecules at equilibrium (black distributions) and prior to oxidation reactions (red distributions). The equilibrium distributions were calculated from intact cyclohexene molecules in the first 50 ps of simulation during which no mechanical stress was applied. The red distributions were calculated from intact cyclohexene molecules that were within 5 ps of participating in an oligomerization reaction. The blue dotted lines show the difference between the red (pre-reaction) and black (equilibrium) distributions.

References

1. Xu, C., De, S., Balu, A. M., Ojeda, M. & Luque, R. Mechanochemical synthesis of advanced nanomaterials for catalytic applications. *Chem. Commun.* **51**, 6698–6713 (2015).
2. Willis-Fox, N., Rognin, E., Aljohani, T. A. & Daly, R. Polymer Mechanochemistry: Manufacturing Is Now a Force to Be Reckoned With. *Chem* **4**, 2499–2537 (2018).
3. Howard, J. L., Cao, Q. & Browne, D. L. Mechanochemistry as an emerging tool for molecular synthesis: what can it offer? *Chem. Sci.* **9**, 3080–3094 (2018).
4. Andersen, J. & Mack, J. Mechanochemistry and organic synthesis: from mystical to practical. *Green Chem.* **20**, 1435–1443 (2018).
5. Do, J.-L. & Friščić, T. Mechanochemistry: A Force of Synthesis. *ACS Cent Sci* **3**, 13–19 (2017).
6. Duwez, A.-S. *et al.* Mechanochemistry: targeted delivery of single molecules. *Nat. Nanotechnol.* **1**, 122–125 (2006).
7. Lee, H., Lee, D. & Jeong, H. Mechanical aspects of the chemical mechanical polishing process: A review. *International Journal of Precision Engineering and Manufacturing* **17**, 525–536 (2016).
8. Ghanem, M. A. *et al.* The role of polymer mechanochemistry in responsive materials and additive manufacturing. *Nature Reviews Materials* **6**, 84–98 (2020).
9. Tysoe, W. On Stress-Induced Tribochemical Reaction Rates. *Tribol. Lett.* **65**, 48 (2017).
10. Spikes, H. Stress-augmented thermal activation: Tribology feels the force. *Friction* **6**, 1–31 (2018).
11. Bell, G. I. Models for the specific adhesion of cells to cells. *Science* **200**, 618–627 (1978).
12. Cao, Z., Zhao, W., Liang, A. & Zhang, J. A general engineering applicable superlubricity: Hydrogenated amorphous carbon film containing nano Diamond particles. *Adv. Mater. Interfaces* **4**, 1601224 (2017).
13. Furlong, O. J., Miller, B. P., Kotvis, P. & Tysoe, W. T. Low-temperature, shear-induced tribofilm formation from dimethyl disulfide on copper. *ACS Appl. Mater. Interfaces* **3**, 795–800 (2011).
14. Boscoboinik, A., Olson, D., Adams, H., Hopper, N. & Tysoe, W. T. Measuring and modelling mechanochemical reaction kinetics. *Chem. Commun.* **56**, 7730–7733 (2020).
15. Davis, D. A. *et al.* Force-induced activation of covalent bonds in mechanoresponsive polymeric materials. *Nature* **459**, 68–72 (2009).
16. Kariyawasam, L. S., Filbin, C., Locke, C. & Yang, Y. From Mechanochemistry to Mechanoresponsive Materials. *Smart Stimuli-Responsive Polymers, Films, and Gels* 1–52 Preprint at https://doi.org/10.1002/9783527832385.ch1 (2022).
17. Clausen-Schaumann, H., Seitz, M., Krautbauer, R. & Gaub, H. E. Force spectroscopy with single bio-molecules. *Curr. Opin. Chem. Biol.* **4**, 524–530 (2000).
18. Rana, R., Hopper, N., Sidoroff, F. & Tysoe, W. T. Critical stresses in mechanochemical reactions. *Chem. Sci.* **13**, 12651–12658 (2022).

19. Wang, Y. *et al.* Pressure-Induced Diels-Alder Reactions in C6 H6 -C6 F6 Cocrystal towards Graphane Structure. *Angew. Chem. Int. Ed Engl.* **58**, 1468–1473 (2019).
20. Zholdassov, Y. S. *et al.* Acceleration of Diels-Alder reactions by mechanical distortion. *Science* **380**, 1053–1058 (2023).
21. Gossweiler, G. R., Kouznetsova, T. B. & Craig, S. L. Force-rate characterization of two spiropyran-based molecular force probes. *J. Am. Chem. Soc.* **137**, 6148–6151 (2015).
22. Sommer, M. Substituent Effects Control Spiropyran-Merocyanine Equilibria and Mechanochromic Utility. *Macromol. Rapid Commun.* **42**, 2000597 (2021).
23. Bustamante, C., Chemla, Y. R., Forde, N. R. & Izhaky, D. Mechanical processes in biochemistry. *Annu. Rev. Biochem.* **73**, 705–748 (2004).
24. Black, A. L., Lenhardt, J. M. & Craig, S. L. From molecular mechanochemistry to stress-responsive materials. *J. Mater. Chem.* **21**, 1655–1663 (2011).
25. Makarov, D. E. Perspective: Mechanochemistry of biological and synthetic molecules. *J. Chem. Phys.* **144**, 030901 (2016).
26. Baláž, P. High-Energy Milling. in *Mechanochemistry in Nanoscience and Minerals Engineering* (ed. Baláž, P.) 103–132 (Springer Berlin Heidelberg, Berlin, Heidelberg, 2008).
27. Tan, D. & Frišcic, T. Mechanochemically Enhanced Organic Transformations. *Sustainable Catalysis: Energy-Efficient Reactions and Applications* 155–182 (2018).
28. Jacobs, T. D. B. & Carpick, R. W. Nanoscale wear as a stress-assisted chemical reaction. *Nat. Nanotechnol.* **8**, 108–112 (2013).
29. Gosvami, N. N. *et al.* Tribology. Mechanisms of antiwear tribofilm growth revealed in situ by single-asperity sliding contacts. *Science* **348**, 102–106 (2015).
30. Fang, L., Korres, S., Lamberti, W. A., Webster, M. N. & Carpick, R. W. What stress components drive mechanochemistry? A study of ZDDP tribofilm formation. *Faraday Discuss.* **241**, 394–412 (2023).
31. Zhang, J. & Spikes, H. On the Mechanism of ZDDP Antiwear Film Formation. *Tribol. Lett.* **63**, 24 (2016).
32. Moino, C., Artusio, F. & Pisano, R. Shear stress as a driver of degradation for protein-based therapeutics: More accomplice than culprit. *Int. J. Pharm.* **650**, 123679 (2024).
33. Zhang, J., Ewen, J. P., Ueda, M., Wong, J. S. S. & Spikes, H. A. Mechanochemistry of Zinc Dialkyldithiophosphate on Steel Surfaces under Elastohydrodynamic Lubrication Conditions. *ACS Appl. Mater. Interfaces* **12**, 6662–6676 (2020).
34. Ernens, D. *et al.* Characterization of the Adsorption Mechanism of Manganese Phosphate Conversion Coating Derived Tribofilms. *Tribol. Lett.* **66**, 131 (2018).
35. Yeon, J., He, X., Martini, A. & Kim, S. H. Mechanochemistry at Solid Surfaces: Polymerization of Adsorbed Molecules by Mechanical Shear at Tribological Interfaces. *ACS Appl. Mater. Interfaces* **9**, 3142–3148 (2017).
36. He, X. & Kim, S. H. Mechanochemistry of Physisorbed Molecules at Tribological Interfaces: Molecular Structure Dependence of Tribochemical Polymerization. *Langmuir* **33**, 2717–2724 (2017).
37. He, X., Barthel, A. J. & Kim, S. H. Tribochemical synthesis of nano-lubricant films from adsorbed molecules at sliding solid interface: Tribo-polymers from α-pinene, pinane, and n-decane. *Surf. Sci.* **648**, 352–359 (2016).

38. Khajeh, A., He, X., Yeon, J., Kim, S. H. & Martini, A. Mechanochemical Association Reaction of Interfacial Molecules Driven by Shear. *Langmuir* **34**, 5971–5977 (2018).
39. He, X., Pollock, A. & Kim, S. H. Effect of Gas Environment on Mechanochemical Reaction: A Model Study with Tribo-Polymerization of α-Pinene in Inert, Oxidative, and Reductive Gases. *Tribology Letters* **67**, 1–9 (2019).
40. He, X., Ngo, D. & Kim, S. H. Mechanochemical Reactions of Adsorbates at Tribological Interfaces: Tribopolymerizations of Allyl Alcohol Coadsorbed with Water on Silicon Oxide. *Langmuir* **35**, 15451–15458 (2019).
41. Gosvami, N. N., Lahouij, I., Ma, J. & Carpick, R. W. Nanoscale in situ study of ZDDP tribofilm growth at aluminum-based interfaces using atomic force microscopy. *Tribol. Int.* **143**, 106075 (2020).
42. Peeters, S., Restuccia, P., Loehlé, S., Thiebaut, B. & Righi, M. C. Tribochemical Reactions of MoDTC Lubricant Additives with Iron by Quantum Mechanics/Molecular Mechanics Simulations. *J. Phys. Chem. C* **124**, 13688–13694 (2020).
43. Righi, M. C., Loehlé, S., de Barros Bouchet, M. I., Philippon, D. & Martin, J. M. Trimethyl-phosphite dissociative adsorption on iron by combined first-principle calculations and XPS experiments. *RSC Adv.* **5**, 101162–101168 (2015).
44. Loehlé, S. & Righi, M. C. First principles study of organophosphorus additives in boundary lubrication conditions: Effects of hydrocarbon chain length. *Lubr. Sci.* **29**, 485–491 (2017).
45. Osei-Agyemang, E., Berkebile, S. & Martini, A. Decomposition Mechanisms of Anti-wear Lubricant Additive Tricresyl Phosphate on Iron Surfaces Using DFT and Atomistic Thermodynamic Studies. *Tribol. Lett.* **66**, 48 (2018).
46. Bettens, T., Alonso, M., Geerlings, P. & De Proft, F. Implementing the mechanical force into the conceptual DFT framework: understanding and predicting molecular mechanochemical properties. *Phys. Chem. Chem. Phys.* **21**, 7378–7388 (2019).
47. Li, Z. & Szlufarska, I. Physical Origin of the Mechanochemical Coupling at Interfaces. *Phys. Rev. Lett.* **126**, 076001 (2021).
48. Senftle, T. P. *et al.* The ReaxFF reactive force-field: development, applications and future directions. *npj Computational Materials* **2**, 1–14 (2016).
49. Martini, A., Eder, S. J. & Dörr, N. Tribochemistry: A Review of Reactive Molecular Dynamics Simulations. *Lubricants* **8**, 44 (2020).
50. Bhuiyan, F. H., Kim, S. H. & Martini, A. Reactive molecular dynamics simulations of thermal and shear-driven oligomerization. *Appl. Surf. Sci.* **591**, 153209 (2022).
51. Khajeh, A. *et al.* Thermal Decomposition of Tricresyl Phosphate on Ferrous Surfaces. *J. Phys. Chem. C* **125**, 5076–5087 (2021).
52. Ayestarán Latorre, C. *et al.* Mechanochemistry of phosphate esters confined between sliding iron surfaces. *Communications Chemistry* **4**, 1–11 (2021).
53. Mohammadtabar, K., Eder, S. J., Bedolla, P. O., Dörr, N. & Martini, A. Reactive Molecular Dynamics Simulations of Thermal Film Growth from Di- tert-butyl Disulfide on an Fe(100) surface. *Langmuir* **34**, 15681–15688 (2018).
54. Mohammadtabar, K., Eder, S. J., Dörr, N. & Martini, A. Heat-, load-, and shear-driven reactions of Di-tert-butyl disulfide on Fe(100). *J. Phys. Chem. C Nanomater. Interfaces* **123**, 19688–19692 (2019).

55. Wen, J. *et al.* Atomic insight into tribochemical wear mechanism of silicon at the Si/SiO2 interface in aqueous environment: Molecular dynamics simulations using ReaxFF reactive force field. *Appl. Surf. Sci.* **390**, 216–223 (2016).
56. Yue, D.-C. *et al.* Tribochemical mechanism of amorphous silica asperities in aqueous environment: a reactive molecular dynamics study. *Langmuir* **31**, 1429–1436 (2015).
57. Wen, J., Ma, T., Zhang, W., van Duin, A. C. T. & Lu, X. Atomistic mechanisms of Si chemical mechanical polishing in aqueous H2O2: ReaxFF reactive molecular dynamics simulations. *Comput. Mater. Sci.* **131**, 230–238 (2017).
58. Hahn, S. H., Liu, H., Kim, S. H. & Duin, A. C. T. Atomistic understanding of surface wear process of sodium silicate glass in dry versus humid environments. *J. Am. Ceram. Soc.* **103**, 3060–3069 (2020).
59. He, H. *et al.* Friction-induced subsurface densification of glass at contact stress far below indentation damage threshold. *Acta Mater.* **189**, 166–173 (2020).
60. Martini, A. & Kim, S. H. Activation Volume in Shear-Driven Chemical Reactions. *Tribol. Lett.* **69**, 150 (2021).
61. Takacs, L. What is unique about mechanochemical reactions? *Acta Phys. Pol. A* **126**, 1040–1043 (2014).
62. Ogbomo, E., Bhuiyan, F. H., Latorre, C. A., Martini, A. & Ewen, J. P. Effects of surface chemistry on the mechanochemical decomposition of tricresyl phosphate. *Phys. Chem. Chem. Phys.* **26**, 278–292 (2023).
63. Chipara, A. C. *et al.* Underwater adhesive using solid–liquid polymer mixes. *Materials Today Chemistry* **9**, 149–157 (2018).
64. Srinivasan, S. G. & van Duin, A. C. T. Molecular-dynamics-based study of the collisions of hyperthermal atomic oxygen with graphene using the ReaxFF reactive force field. *J. Phys. Chem. A* **115**, 13269–13280 (2011).
65. Chenoweth, K., van Duin, A. C. T. & Goddard, W. A., 3rd. ReaxFF reactive force field for molecular dynamics simulations of hydrocarbon oxidation. *J. Phys. Chem. A* **112**, 1040–1053 (2008).
66. Chenoweth, K., Cheung, S., van Duin, A. C. T., Goddard, W. A., 3rd & Kober, E. M. Simulations on the thermal decomposition of a poly(dimethylsiloxane) polymer using the ReaxFF reactive force field. *J. Am. Chem. Soc.* **127**, 7192–7202 (2005).
67. Plimpton, S. Fast Parallel Algorithms for Short-Range Molecular Dynamics. *J. Comput. Phys.* **117**, 1–19 (1995).
68. Stukowski, A. Visualization and analysis of atomistic simulation data with OVITO–the Open Visualization Tool. *Modell. Simul. Mater. Sci. Eng.* **18**, 015012 (2009).
69. Menzinger, M. & Wolfgang, R. The meaning and use of the Arrhenius activation energy. *Angew. Chem. Int. Ed Engl.* **8**, 438–444 (1969).
70. Zhang, J., Ewen, J. P. & Spikes, H. A. Substituent effects on the mechanochemical response of zinc dialkyldithiophosphate. *Molecular Systems Design & Engineering* (2022) doi:10.1039/D2ME00049K.
71. Ewen, J. P. *et al.* Substituent Effects on the Thermal Decomposition of Phosphate Esters on Ferrous Surfaces. *J. Phys. Chem. C* **124**, 9852–9865 (2020).
72. Smidstrup, S. *et al.* QuantumATK: an integrated platform of electronic and atomic-scale modelling tools. *J. Phys. Condens. Matter* **32**, 015901 (2020).
73. Koo, B., Nofen, E., Chattopadhyay, A. & Dai, L. Dimeric anthracene-based mechanophore for damage precursor detection in epoxy-based thermoset polymer

matrix: Characterization and atomistic modeling. *Comput. Mater. Sci.* **133**, 167–174 (2017).
74. Brown, C. L. *et al.* Substituent Effects in Mechanochemical Allowed and Forbidden Cyclobutene Ring-Opening Reactions. *J. Am. Chem. Soc.* **143**, 3846–3855 (2021).
75. Pill, M. F. *et al.* Mechanochemical Cycloreversion of Cyclobutane Observed at the Single Molecule Level. *Chemistry* **22**, 12034–12039 (2016).
76. Pawlak, R. *et al.* Sequential Bending and Twisting around C-C Single Bonds by Mechanical Lifting of a Pre-Adsorbed Polymer. *Nano Lett.* **20**, 652–657 (2020).
77. Lavoie, S. R., Long, R. & Tang, T. Modeling the Mechanics of Polymer Chains with Deformable and Active Bonds. *J. Phys. Chem. B* **124**, 253–265 (2020).
78. Chen, B., Hoffmann, R. & Cammi, R. The Effect of Pressure on Organic Reactions in Fluids-a New Theoretical Perspective. *Angew. Chem. Int. Ed Engl.* **56**, 11126–11142 (2017).
79. Chen, B., Houk, K. N. & Cammi, R. High-Pressure Reaction Profiles and Activation Volumes of 1,3-Cyclohexadiene Dimerizations Computed by the Extreme Pressure-Polarizable Continuum Model (XP-PCM). *Chemistry* **28**, e202200246 (2022).
80. Ong, M. T., Leiding, J., Tao, H., Virshup, A. M. & Martínez, T. J. First principles dynamics and minimum energy pathways for mechanochemical ring opening of cyclobutene. *J. Am. Chem. Soc.* **131**, 6377–6379 (2009).
81. Wollenhaupt, M., Krupička, M. & Marx, D. Should the Woodward-Hoffmann Rules be Applied to Mechanochemical Reactions? *Chemphyschem* **16**, 1593–1597 (2015).
82. Ribas-Arino, J., Shiga, M. & Marx, D. Understanding covalent mechanochemistry. *Angew. Chem. Int. Ed Engl.* **48**, 4190–4193 (2009).
83. Koo, B., Chattopadhyay, A. & Dai, L. Atomistic modeling framework for a cyclobutane-based mechanophore-embedded nanocomposite for damage precursor detection. *Comput. Mater. Sci.* **120**, 135–141 (2016).
84. Bhuiyan, F. H., Li, Y.-S., Kim, S. H. & Martini, A. Shear-activated chemisorption and association of cyclic organic molecules. *Faraday Discuss.* **241**, 194–205 (2023).
85. Li, Y.-S., Jang, S., Bhuiyan, F. H., Martini, A. & Kim, S. H. Molecular Structure and Environment Dependence of Shear-Driven Chemical Reactions: Tribopolymerization of Methylcyclopentane, Cyclohexane and Cyclohexene on Stainless Steel. *Tribol. Lett.* **71**, 49 (2023).
86. Mozzi, R. L. & Warren, B. E. The structure of vitreous silica. *J. Appl. Crystallogr.* **2**, 164–172 (1969).
87. Da Silva, J. R. G., Pinatti, D. G., Anderson, C. E. & Rudee, M. L. A refinement of the structure of vitreous silica. *The Philosophical Magazine: A Journal of Theoretical Experimental and Applied Physics* **31**, 713–717 (1975).
88. Zhuravlev, L. T. The surface chemistry of amorphous silica. Zhuravlev model. *Colloids Surf. A Physicochem. Eng. Asp.* **173**, 1–38 (2000).
89. Berne, B. J., Ciccotti, G. & Coker, D. F. *Classical And Quantum Dynamics In Condensed Phase Simulations: Proceedings Of The International School Of Physics*. (World Scientific, 1998).
90. Henkelman, G. & Jónsson, H. Improved tangent estimate in the nudged elastic band method for finding minimum energy paths and saddle points. *J. Chem. Phys.* **113**, 9978–9985 (2000).

91. Nakano, A. A space–time-ensemble parallel nudged elastic band algorithm for molecular kinetics simulation. *Comput. Phys. Commun.* **178**, 280–289 (2008).
92. Maras, E., Trushin, O., Stukowski, A., Ala-Nissila, T. & Jónsson, H. Global transition path search for dislocation formation in Ge on Si(001). *Comput. Phys. Commun.* **205**, 13–21 (2016).
93. Koistinen, O.-P., Ásgeirsson, V., Vehtari, A. & Jónsson, H. Nudged Elastic Band Calculations Accelerated with Gaussian Process Regression Based on Inverse Interatomic Distances. *J. Chem. Theory Comput.* **15**, 6738–6751 (2019).
94. Barthel, A. J. & Kim, S. H. Lubrication by physisorbed molecules in equilibrium with vapor at ambient condition: effects of molecular structure and substrate chemistry. *Langmuir* **30**, 6469–6478 (2014).
95. Ewen, J. P., Spikes, H. A. & Dini, D. Contributions of Molecular Dynamics Simulations to Elastohydrodynamic Lubrication. *Tribol. Lett.* **69**, 24 (2021).
96. Chiang, J. F. & Bauer, S. H. Molecular structure of cyclohexene. *J. Am. Chem. Soc.* **91**, 1898–1901 (1969).
97. Kumar, S., Zeller, F. & Stauch, T. A Two-Step Baromechanical Cycle for Repeated Activation and Deactivation of Mechanophores. *J. Phys. Chem. Lett.* **12**, 9470–9474 (2021).
98. Stauch, T. & Dreuw, A. Knots "Choke Off" Polymers upon Stretching. *Angew. Chem. Int. Ed Engl.* **55**, 811–814 (2016).
99. Bustamante, C., Smith, S. B., Liphardt, J. & Smith, D. Single-molecule studies of DNA mechanics. *Curr. Opin. Struct. Biol.* **10**, 279–285 (2000).
100. Hugel, T. *et al.* Elasticity of Single Polyelectrolyte Chains and Their Desorption from Solid Supports Studied by AFM Based Single Molecule Force Spectroscopy. *Macromolecules* **34**, 1039–1047 (2001).
101. Zhao, L., Zhi, M. & Frenking, G. The strength of a chemical bond. *Int. J. Quantum Chem.* **122**, (2022).
102. Hermann, M. & Frenking, G. The Chemical Bond in C2. *Chemistry* **22**, 4100–4108 (2016).
103. Hoshino, K., Yagishita, K., Tagawa, K. & Spikes, H. Tribological Properties of Sulphur-Free Antiwear Additives Zinc Dialkylphosphates (ZDPs). *SAE International Journal of Fuels and Lubricants; Warrendale* **5**, 504–510 (2012).